Chapter 13
Hydrogen, the Principal Agent of Structural and Chemical Diversity in Minerals

Frank C. Hawthorne

Hydrogen (both neutral H and H^+) is the smallest element in the Periodic Table (Rahm et al. 2017) and small size and high volatility make it perhaps the most widely distributed element on Earth. Despite the fact that H constitutes less than 0.1% of the Earth by mass, it is capable of incorporation into the majority of minerals at a major level. Hydrogen occurs as a required constituent in ~60% of all minerals and plays a variety of roles that give rise to the complexity (sensu lato) and range of structure and chemical composition that is characteristic of oxide and oxysalt minerals in particular. Here I examine the diversity of mechanisms by which H is incorporated in minerals and the various ways in which H promotes stable atomic arrangements. I will use Φ to designate a ligand: $\Phi = O^{2-}$, $(OH)^-$, F^-, Cl^-, $(H_2O)^0$ and I will write a polyhedron most generally as $(M\Phi_n)$ and more specifically by the central cation: thus the expression "Mg^{2+} octahedron" designates an $(Mg\Phi_6)$ octahedron.

13.1 Stereochemistry of H^+

Hydrogen is electropositive and may be considered as a monovalent cation in crystals where it commonly has the coordination number [2]. The geometrical details of the local stereochemistry around the hydrogen atom in inorganic structures have been examined in considerable detail: e.g., Ferraris and Franchini-Angela (1972), Brown (1976), Ferraris and Ivaldi (1984) and Milovanović et al. (2022). Commonly, [2]-coordination of H^+ is very asymmetric: H^+ forms a strong bond with the closer anion and a weak bond with the more distant anion (Fig. 13.1). This arrangement can be written as D–H…A where D is the strongly bonded *donor* anion, A is the weakly bonded *acceptor* anion, and H…A is the *hydrogen bond.* In general, 100 < D–H…A

F. C. Hawthorne (✉)
Earth Sciences, University of Manitoba, Winnipeg, MB R3T 2N2, Canada
e-mail: frank.hawthorne@umanitoba.ca

L. Bindi and G. Cruciani (eds.), *Celebrating the International Year of Mineralogy*,
Springer Mineralogy, https://doi.org/10.1007/978-3-031-28805-0_13

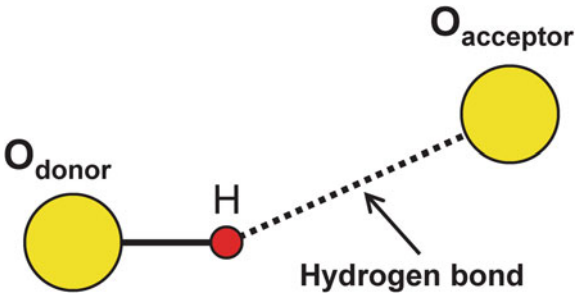

Fig. 13.1 The geometry and nomenclature of the hydrogen bond. Large yellow circles: O^{2-} ions; small red circle: H^+ ion; full black line: $O^{2-}{}_{donor}$–H^+ bond; dotted black line: hydrogen bond

$\leq 180°$ with an average value of ~165°; large angles (~180°) are usually characteristic of strong hydrogen bonds (Brown 1976). Coordination numbers greater than [2] do occur for H^+ in minerals although they are much less common than [2]: there is one short D–H bond and two (or more) weak H…A hydrogen bonds, usually designated as *bifurcated* (or *trifurcated)* hydrogen bonds.

13.2 Bond-Valence Theory

Bond-valence theory (Brown 2002, 2016; Hawthorne 2012, 2015) is a theory of atom–atom interactions in atomic arrangements. It is a back-of-the-envelope method in which physical details are not obscured by complexities of computation, and can be used for very complicated minerals with considerable chemical and structural disorder (e.g., byzantievite: $Ba_5(Ca,REE,Y)_{22}(Ti,Nb)_{18}(SiO_4)_4[(PO_4),(SiO_4)]_4(BO_3)_9O_{22}[(OH),F]_{43}(H_2O)_{1.5}$, Sokolova et al. 2010). For any pair of bonded atoms, *bond valence is a measure of the strength of the bond* and is inversely proportional to the length of the bond. It may be calculated using observed bond-lengths and bond-valence curves of the general form $s_{ij} = \exp[(R_o–R_{ij})/B]$, where s_{ij} is the bond valence between ions i and j, R_{ij} is the observed bond-length, and R_o and B are fitted parameters, e.g., Gagné and Hawthorne (2015) for atom pairs involving O^{2-}, and Brown and Altermatt (1985) for atom pairs involving other simple anions (e.g., Cl^-, F^-).

13.2.1 Lewis Acids and Lewis Bases

Brown (2002, 2016) defined the *Lewis-acid strength* of a cation as its characteristic bond-valence, which is equal to its atomic (formal) valence divided by its mean coordination-number; a comprehensive set of values is given by Gagné and Hawthorne (2017) based on ~10,000 well-refined crystal-structures. The Lewis-base strength of an anion is defined as the characteristic valence of the bonds formed by the anion. Simple anions, e.g., O^{2-}, F^-, exhibit an extremely wide range of bond valence;

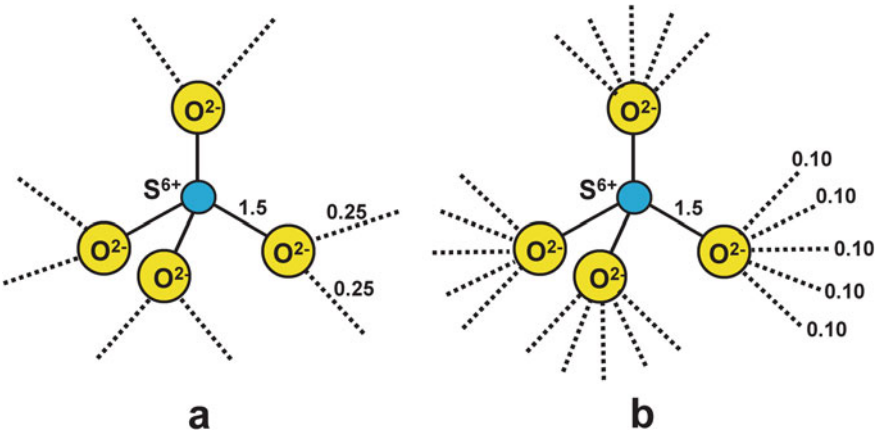

Fig. 13.2 The bond-valence structures of the $(SO_4)^{2-}$ polyanion with **a** two additional bonds incident at each O^{2-} ion, and **b** five additional bonds incident at each O^{2-} ion; small blue circles: S^{6+} ions

for example, values for O^{2-} vary from 0.17 *vu* in (NaO_6) polyhedra to 2.0 *vu* in CrO_3 (Stephens and Cruickshank 1970), and Lewis basicities for such simple anions have little or no predictive value. However, high-valence polyanions, e.g., $(SO_4)^{2-}$, exhibit a much more restricted range of Lewis basicity. Figure 13.2 shows the bond-valence structure of the $(SO_4)^{2-}$ polyanion. Most of the bond valence required by each O^{2-} ion of $(SO_4)^{2-}$ is provided by the S^{6+}–O^{2-} bond (at ~1.5 *vu*), and the remainder comes from the cations bonded to the $(SO_4)^{2-}$ polyanion. Two examples are shown here; in Fig. 13.2a, each O^{2-} accepts two additional bonds of 0.25 *vu*, and in Fig. 13.2b, each O^{2-} accepts five additional bonds of 0.10 *vu*. For $M_2(SO_4)$, $M^+ = Na^+$, K^+, Rb^+, Cs^+, and $Mg(SO_4)(H_2O)_n$, $n = 6,7$, the mean number of bonds accepted by the $(SO_4)^{2-}$ polyanion is 3.83×4 and the Lewis basicity is $2/(3.83 \times 4) = 0.13$ *vu*. It is apparent that the range of incident bond-valences possible is far less for the $(SO_4)^{2-}$ polyanion than for the simple O^{2-} ion, and that defining Lewis basicities for polyanions provides useful predictive capability. Values for Lewis basicities of polyanions are given in Table 13.1.

13.2.2 The Basic Axioms of Bond-Valence Theory

Bond-valence theory has three principal axioms: (1) the valence-sum rule; (2) the path (loop) rule; and (3) the valence-matching principle.

The valence-sum rule: *The magnitude of the sum of the bond valences incident at each ion is equal to the magnitude of the valence of that ion.* For any field, the flux theorem of Gauss (Matthews 1998) relates the distribution of electric charge to the resulting electric field: the flux of the field intensity through a closed surface is

Table 13.1 Lewis basicities (*vu*) for oxyanions

$(BO_3)^{3-}$	0.33	$(AsO_4)^{3-}$	0.25
$(BO_2(OH))^{2-}$	0.27	$(AsO_3(OH))^{2-}$	0.19
$(BO_4)^{5-}$	0.42	$(AsO_2(OH)_2)^{-}$	0.13
$(SiO_4)^{4-}$	0.33	$(VO_4)^{3-}$	0.25
$(SiO_3(OH))^{3-}$	0.29	$(VO_3(OH))^{2-}$	0.19
$(SiO_2(OH)_2))^{2-}$	0.23	$(VO_2(OH)_2)^{-}$	0.13
$(AlO_4)^{5-}$	0.42	$(CO_3)^{2-}$	0.22
$(PO_4)^{3-}$	0.25	$(CO_2(OH))^{-}$	0.19
$(PO_3(OH))^{2-}$	0.19	$(NO_3)^{-}$	0.17
$(PO_2(OH)_2)^{-}$	0.13	$(SO_4)^{2-}$	0.13
$(As^{3+}O_3)^{3-}$	0.33	$(SO_3(OH))^{-}$	0.06

related to the total net charge enclosed within that surface. The valence-sum rule is thus a corollary of the flux theorem applied to the electrostatic potential field (Preiser et al. 1999).

The path rule: *The sum of the directed bond-valences along any path between crystallographically equivalent ions in a structure is equal to zero* (Gagné et al. 2018). This definition includes closed paths (loops) as this rule was originally formulated just for loops (Brown 1981).

The valence-matching principle: *For a chemical bond to form, the Lewis acidity (the electron-attracting capacity of the cation) must match the Lewis basicity (electron-donating capacity) of the anion.* This argument is based on the handshaking principle of Graph Theory (e.g., Wilson 1979), and leads to a specific criterion for chemical bonding, the valence-matching principle (Brown 2016): *Stable structures will form where the Lewis-acid strength of the cation closely matches the Lewis-base strength of the anion.*

Bond-valence theory plays a critical role in understanding the different mechanisms involved in incorporating H^+ into mineral structures, in particular because of the disorder that so often accompanies the presence of $(OH)^-$ and $(H_2O)^0$ in minerals.

13.3 The Incorporation of H^+ into Mineral Structures

Hydrogen may be incorporated in mineral structures in the following ways: (1) as strongly bonded complexes involving other first-row ions; (2) as strongly bonded complexes involving oxyions; (3) as an itinerant ion.

13.3.1 *Strongly Bonded Polyions Involving H^+ and Other First-Row Ions*

Hydrogen is strongly bonded to a donor anion, and it is common practice to consider the first-row elements bonded to H^+ as complex species (polyions) or groups. With regard to the Earth, there are four ions of relevance here: C^{4-}, N^{3-}, O^{2-} and F^-. The bonding behaviour of H^+ and F^- is similar to that of the other three first-row ions but HF and $HF(H_2O)$ occur only as fluids at the surface of the Earth, and HF has not been reported as a constituent of a mineral.

There are four different H^+–O^{2-}-bearing groups in oxide and oxysalt minerals: $(OH)^-$, $(H_2O)^0$, $(H_3O)^+$ and $(H_5O_2)^+$ (Fig. 13.3a–d). It is apparent from the typical bond-valence values shown in Fig. 13.3 that the coordination of H^+ is very asymmetric, with common O_{donor}–H bond-valences ranging from 0.90–0.50 *vu* and H…$O_{acceptor}$ bond-valences ranging from 0.10–0.50 *vu*. This behaviour is apparent in the variation of observed O_{donor}–H and H…$O_{acceptor}$ bond-distances (Fig. 13.4a) which show a very strong bimodal distribution with maxima at 0.983 Å for O_{donor}–H bonds and 1.764 Å for H…$O_{acceptor}$ bonds (Gagné and Hawthorne 2018). There is also a weak third maximum at 1.236 Å that corresponds approximately to the length of a symmetrical hydrogen-bond. There is a very strong correlation between the H…$O_{acceptor}$ distance and the O_{donor}–H distance for $^{[2]}H^+$ (Fig. 13.4b). The solid line in Fig. 13.4b was calculated with the H^+–O^{2-} bond-valence parameters of Gagné and

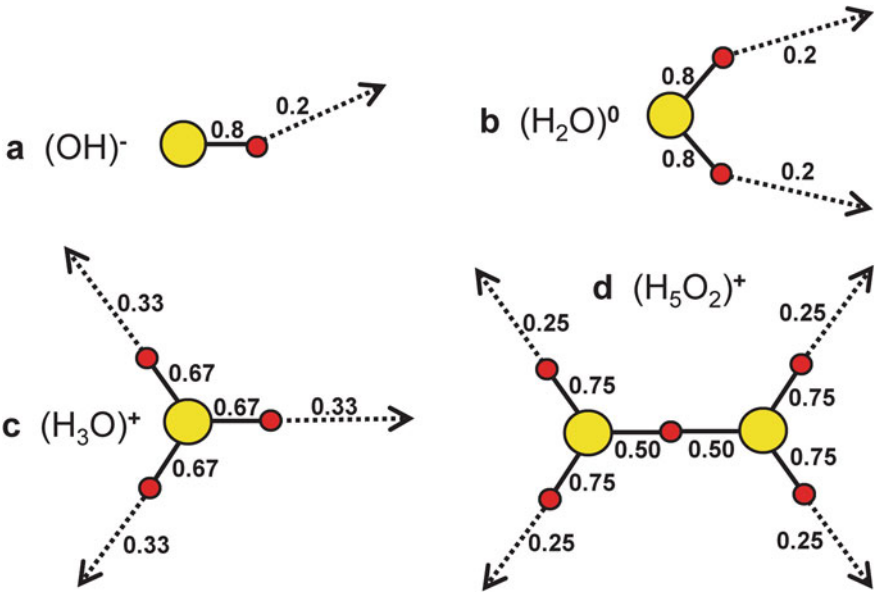

Fig. 13.3 The geometry and typical bond-valence structures of hydrogen-bearing groups in minerals: **a** $(OH)^-$; **b** $(H_2O)^0$; **c** $(H_3O)^+$; **d** $(H_5O_2)_+$; bond-valence values in *vu* (valence units)

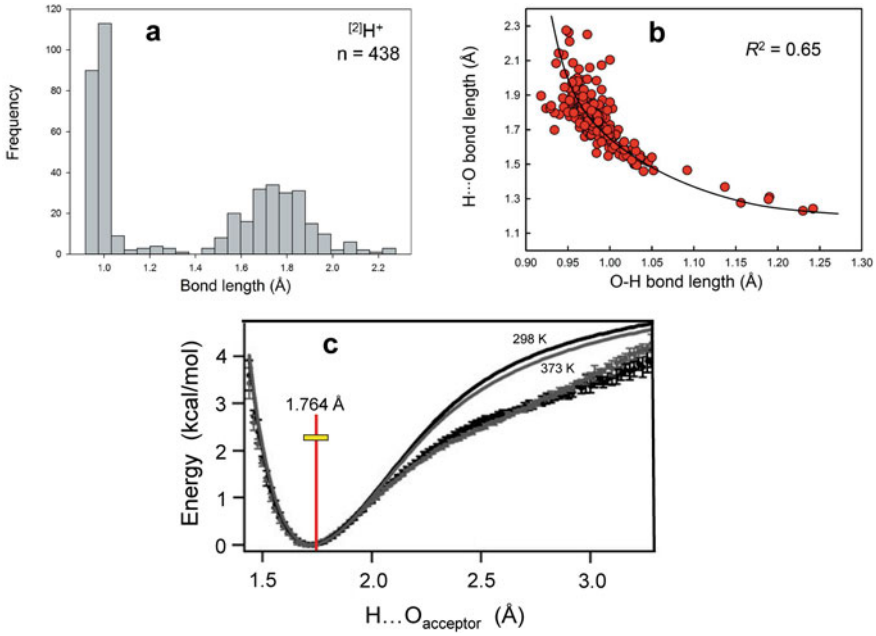

Fig. 13.4 **a** Bond-length variation for $^{[2]}H^{+}$ bonded to O^{2-} in inorganic structures; **b** variation of H…$O_{acceptor}$ hydrogen-bond distance as a function of the O_{donor}–H distance for $^{[2]}H^{+}$. The solid line shows accord with the valence-sum rule for the bond-valence parameters of Gagné and Hawthorne (2015). **c** Calculated energy of hydrogen-bond distortion as a function of H…$O_{acceptor}$ distance at T = 298 and 373 K. Continuous lines: H…$O_{acceptor}$ pair energy; discontinuous data: system energy. All functions are shifted to have a common minimum energy of zero; the red line indicates the mean H…$O_{acceptor}$ distance in minerals (see text). (a) and (b) modified from Gagné and Hawthorne (2018); (c) modified from Smith et al. (2005)

Hawthorne (2015) and shows accord with the valence-sum rule of Brown (2016), indicating that the H^{+}–O^{2-} interaction may be described adequately by a single set of bond-valence parameters across the whole range of observed distances. Moreover, the grand mean observed H…$O_{acceptor}$ distance of 1.764 Å with a standard deviation of 0.156 Å (red line and yellow box in Fig. 13.4c) is close to the minimum-energy H…$O_{acceptor}$ distance calculated for water (Fig. 13.4c) by Smith et al. (2005).

Positively-charged groups involving H^{+} and O^{2-} act as polycations although they are extremely uncommon in minerals (Table 13.1). They have been identified in hydronium jarosite $\{H_3O\}[Fe^{2+}{}_3(SO_4)_2(OH)_6]$, Ripmeester et al. (1986); rhomboclase $\{H_5O_2\}[Fe^{3+}(SO_4)_2(H_2O)_2]$, Mereiter 1974); mejillonesite $(H_5O_2)NaMg_2(PO_3OH)(PO_4)(OH)$, Atencio et al. (2012). Larger arrangements of donor anions and H^{+} ions have been noted in synthetic inorganic crystals, e.g., $(H_7O_2)^{3+}$, $(H_{14}O_6)^{2+}$; Emsley et al. (1981), but these cannot be considered as strongly bonded complexes as their internal bonds must include (weak) hydrogen bonds as integral linkages of the arrangements.

There are two H^+–N^{3-}-bearing groups in oxide and oxysalt minerals: $(NH_3)^0$ and $(NH_4)^+$ (Fig. 13.5). As $(NH_3)^0$ is a neutral group, it may occur as (1) an occluded group where it is trapped in a cavity in a structure but not bonded to any of the surrounding ions (Fig. 13.5a); as the N^{3-} ion lies to one side of its coordinating H^+ ions, (2) N^{3-} may bond to a cation in the structure, and the valence-sum rule will then give rise to hydrogen bonds to other anions in the structure (Fig. 13.5b). This latter arrangement is seen in shilovite, Fig. 13.5c, $Cu(NH_3)_4(NO_3)_2$, Chukanov et al. 2015). In the $(NH_4)^+$ group, the tetrahedron of H^+ ions surround the central N^{3-} ion and prevents any other cation from bonding to N^{3-}, and $(NH_4)^+$ acts as a polycation (Fig. 13.5d). There are two H^+–C^{4-}-bearing groups in oxide and oxysalt minerals: $(CH_3)^{-1}$ is pyramidal (Fig. 13.6a) and bonds to other ions in a structure whereas $(CH_4)^0$ (Fig. 13.6b) is neutral and may occur only as an occluded group where it is trapped in a cavity in a structure. Their frequencies of occurrence as dominant polyions in minerals are summarized in Table 13.2; note that where there is solid solution of F^- for $(OH)^-$, many additional minerals will contain substantial but non-essential $(OH)^-$, increasing the number of mineral species with significant $(OH)^-$ content.

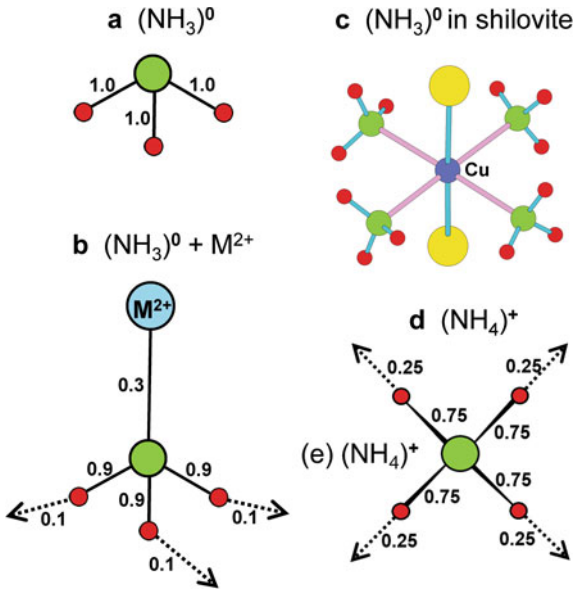

Fig. 13.5 The bond-valence structures of the $(NH_3)^0$ and $(NH_4)^+$ polyions: **a** the $(NH_3)^0$ group; **b** sketch of the $(NH_3)^0$ group with N^{3-} bonded to an M^{2+} ion; **c** an example of (b) in the structure of shilovite (Chukanov et al. 2015), Cu^{2+} coordinated by four $(NH_3)^0$ groups and two O^{2-} ions; **d** $(NH_4)^+$ polyion. Green circle: N^{3-} ion; dark-blue circle: Cu^{2+} ion

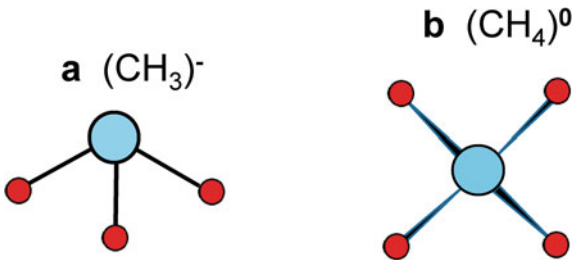

Fig. 13.6 The bond-valence structures of the $(CH_3)^-$ and $(CH_4)^0$ polyions: **a** the $(CH_3)^-$ group; **b** the $(CH_4)^0$ group. Large blue circles: C^{4-} ions

Table 13.2 Numbers of minerals containing specific H-bearing complexes

H-bearing complex	Number of minerals	% of minerals
$(OH)^-$	1021	20.02
$(H_2O)^0$	823	16.14
$(OH)^- + (H_2O)^0$	1004	19.69
$(H_3O)^+$	16	0.31
$(NH_4)^+$	154	3.02
$SO_3(OH)$	9	0.18
$PO_3(OH)$	66	1.29
$PO_2(OH)_2$	2	0.04
$AsO_3(OH)$	57	1.12
$AsO_2(OH)_2$	5	0.10
$SiO_3(OH)$	23	0.45
$CO_2(OH)$	9	0.18
$As(OH)_3$	1	0.02

13.3.2 Strongly Bonded Polyions Involving H^+ and High-Valence Oxyanions

The bond-valence requirements of high-valence-oxyanion minerals are dominated by the oxyanion and its polymerization, in accord with the definition and organization of structure hierarchies of minerals (Hawthorne 2014). Of particular interest with regard to minerals are linkages between H^+ and $(TO_4)^{n-}$ and $(TO_3)^{n-}$ groups where $^{[4]}T = S^{6+}, P^{5+}, As^{5+}, V^{5+}$ and Si^{4+}, and $^{[3]}T = As^{3+}, B^{3+}$ and C^{4+}. The atomic arrangements of these $(TO_{4-n}(OH)_n)$ and $(TO_{3-n}(OH)_n)$ groups occurring in minerals are shown in Fig. 13.7a–d and their chemical compositions are listed in Table 13.2 together with their frequencies of occurrence.

There are two situations with regard to the occurrence of these groups in minerals:

(1) H^+ will bond to a ligand of $^{[3]}T$ or $^{[4]}T$ where the general arrangement of coordination polyhedra is such that there is not a cation of sufficient Lewis acidity close enough to bond to that ligand and satisfy its bond-valence requirements.

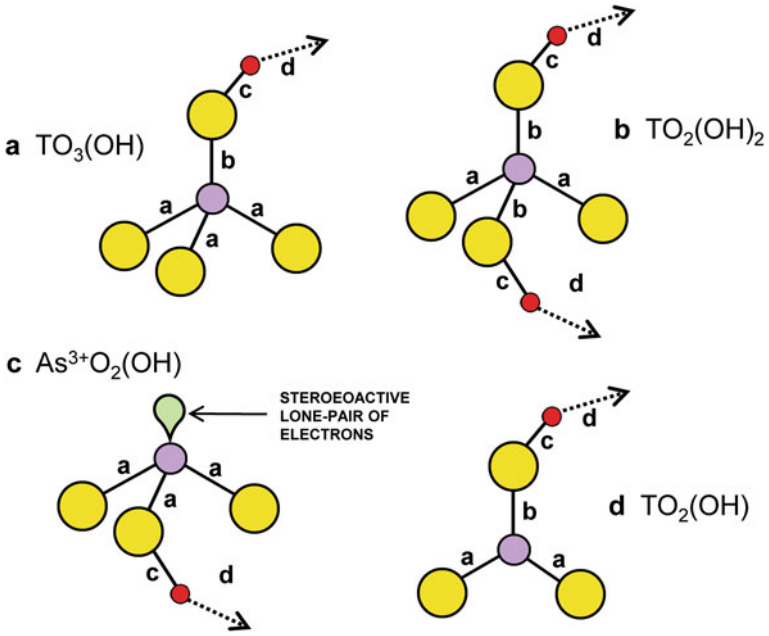

Fig. 13.7 The atomic arrangements of $(TO_{4-n}(OH)_n)$ and $(TO_{3-n}(OH)_n)$ groups in minerals: **a** $TO_3(OH)$; **b** $TO_2(OH)_2$; **c** $As^{3+}O_2(OH)$; **d** $TO_2(OH)$. Small mauve circles: T atoms

This situation may be accommodated by the ligand acting as an O_{donor} ion for H^+, forming an $(OH)^-$ group and an acid oxyanion: e.g., $(T^{5+}O_3(OH)^-)^{2-}$.

(2) The protonated (acid) oxyanion occurs in aqueous solution, e.g., $(CO_2(OH))^-$, and may retain its identity upon crystallization.

Many of the polyanions listed in Table 13.1 occur as complexes in aqueous solution, suggesting a link between the aqueous complexes and the atomic arrangements of the minerals that crystallize from such solutions. I will use the following definitions: (1) (H_2O) is a group or molecule; (2) water is a liquid of chemical composition $\sim(H_2O)_n$; (3) ice is a solid phase of chemical composition $\sim(H_2O)_n$. I use the term H_2O to refer to the chemical composition of H_2O, and (H_2O) to refer to the group in an extended crystal structure. Why be so specific about this? Because the physical states and the resulting physical properties of ice, water and vapour are different (away from critical points), and their roles in Earth processes are also different.

H_2O is amphoteric: it can act as an acid and as a base. Water dissociates via the following reaction:

$$2H_2O = (H_3O)^+ + (OH)^-$$

and pH is inversely related to the activity of the H^+ ion in solution. Where pH is low (below ~7), the activity of H^+ is high and represented by the presence of $(H_3O)^+$;

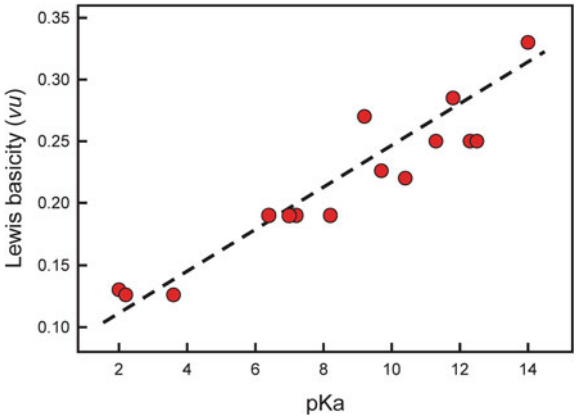

Fig. 13.8 Lewis basicity of some polyanions in Table 13.1 versus pK_a of the corresponding polyprotic acid

where pH is high (greater than ~7), the activity of H^+ is low and represented by the presence of $(OH)^-$. Many of the Lewis bases of Table 13.1 exist as complexes in aqueous solution and the crystallization of minerals from aqueous solution may be summarized by the reaction acid + base = salt + water. The base in solution is controlled by the dissociation of the corresponding acid. Where the acid is polyprotic (has more than one proton), a sequence of dissociations occurs, e.g.:

$$H_3PO_4 \rightleftharpoons (PO_2(OH)_2)^- + H^+, \ pK_{a1} = 2.2$$

$$H_2PO_4^- \rightleftharpoons (PO_3(OH))^{2-} + H^+, \ pK_{a2} = 7.2$$

$$HPO_4^{2-} \rightleftharpoons (PO_4)^{3-} + H^+, \ pK_{a3} = 12.3$$

where pK_{an} is the negative log of the nth acid-dissociation constant. The base reaches its maximum concentration in solution at a pH midway between the two bounding pKa values (from Perrin 1965). Thus one expects a correlation between pKa and the Lewis basicity (Table 13.1) of the corresponding polyanion. Figure 13.8 shows that this is indeed the case. As the polyanion is stable over a range of pH, the assigned Lewis basicity will be an average value over this range. Moreover, pK_a is also dependent on temperature, and detailed analysis of crystallization-dissolution relations will need to take this dependency into account.

13.3.3 Itinerant Protons

The H^+ ion, or proton, has a much higher diffusion rate than other cations of the same charge (Table 13.3, data from https://en.wikipedia.org/wiki/Grotthuss_mechanism). As a consequence, H^+ is an important catalyst in many mineral reactions and also

strongly effects the physical properties of minerals. In particular, it often shows dynamic disorder as in the examples given below.

The crystal structure of vesuvianite is most generally written as $X_{19}Y_{13}T_5Z_{18}O_{68}W_{10}$ (Groat et al. 1992a) where X = Ca, Na, REE, Pb^{2+}, Sb^{3+}; Y = Al, Mg, Fe^{2+}, Fe^{3+}, Mn^{2+}, Ti^{4+}, Cr^{3+}, Cu^{2+}, Zn; T = O, B; Z = Si; W = (OH), F, O. In this rather complicated structure (Groat et al. 1992b), H^+ occurs both in the bulk of the structure and in channels down the **c**-axis. The arrangement of H^+ in the channels is shown in Fig. 13.9a. The H^+ ion labelled H2 has O(10) as both donor and acceptor anions, and crystal-structure refinement shows it to be disordered about a centre of symmetry halfway between the two O(10) locations. As the bond-valence requirement of H^+ is not satisfied where either of the locally associated O(1) anions is the donor anion, it seems likely that H^+ hops between the two off-centre H2 positions in a vain attempt to improve its accord with the valence-sum rule. Infrared spectra of this vesuvianite (Fig. 13.9b) show bands from 3700–3400 cm^{-1} due to H^+ in the bulk of the structure and bands from 3200–3000 cm^{-1} due to H^+ in the channel. At room temperature, the 3200 cm^{-1} band has a long tail to ~2900 cm^{-1}, unlike bands due to localised H^+ at 3700–3400 cm^{-1}, and is partly resolved into three bands at liquid-nitrogen temperature, suggesting that the long tail at room

Table 13.3 Diffusion rates of ions in an electric field

Ion	Mobility*
H^+	3.620
NH_4^+	0.763
K^+	0.762
Na^+	0.519
* $\times 10^{-3}/cm^2V^{-1}\ s^{-1}$	

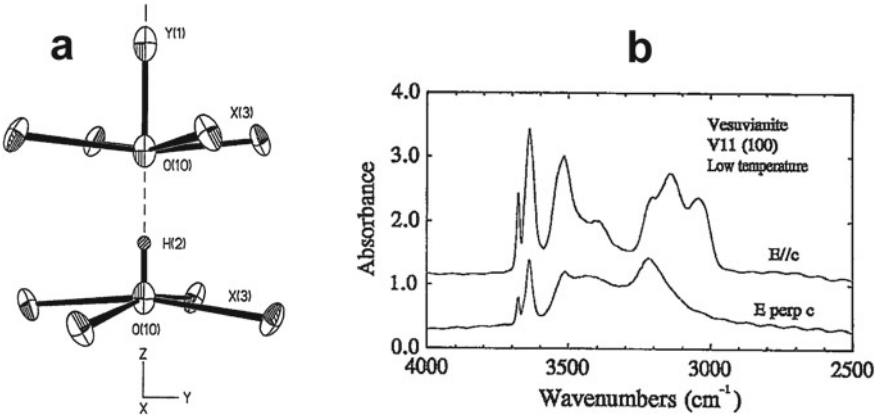

Fig. 13.9 **a** The arrangement of H^+ and associated ions in the channels of the vesuvianite structure (modified from Groat et al. 1992b); **b** polarized infrared spectra in the principal (OH)-stretching region for vesuvianite at liquid-nitrogen temperature (modified from Groat et al. 1995)

temperature is due to a spectrum of environments associated with hopping of the proton, and the three absorptions at low temperature are due to partial inhibition of hopping.

The crystal structure of schwartzemburgite, $Pb^{2+}{}_5I^{3+}O_6Cl_3H_2$ Welch et al. (2001), consists of sheets of composition $[(Pb^{2+}{}_5I^{3+})O^{2-}{}_6]^+$ similar to the structure of tetragonal PbO with every sixth Pb^{2+} replaced by I^{3+}, intercalated with sheets of Cl^- ions which provide additional coordination to the Pb^{2+} ions. Electroneutrality is maintained in the structure by the inclusion of $H^+{}_2$, but there are no anions that have sufficient deficiency in bond valence to act as donor anions to H^+ which is thus forced to move throughout the structure along the paths of highest anion bond-valence deficiency, suggesting that schwartzemburgite may be an ionic conductor. This behaviour is in accord with the infrared spectrum in the principal (OH)-stretching region (Fig. 13.10a) which shows a fine-structured absorption band with a half-width of ~600 cm^{-1}, close to two orders of magnitude larger than bands for well-ordered $(OH)^-$ ions.

Cámara et al. (2004) reported on the structure of a synthetic (OH)-excess amphibole, $NaNa_2Mg_5Si_8O_{21}(OH)_3$. In the structure, there are no obvious donor anions for the excess H^+ ion as the incident bond-valence sums (ignoring excess H^+) at the available anions are in the range 1.50–2.0 *vu* (Cámara et al. 2004), it seems more likely that the excess proton is itinerant. The infrared spectrum (Fig. 13.10b) shows a very broad peak centered on ~3400 cm^{-1} with a long tail stretching to ~2800 cm^{-1} when adsorbed moisture is removed on heating at 250 °C, somewhat similar to the spectra of vesuvianite and schwartzemburgite. This result is very intriguing with

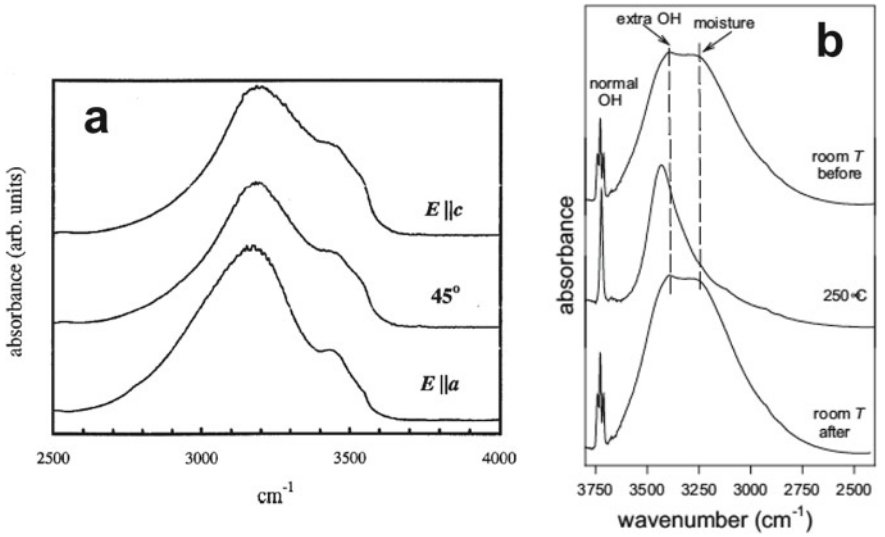

Fig. 13.10 **a** Polarized infrared spectra in the principal (OH)-stretching region for schwartzemburgite (modified from Welch et al. 2001); **b** infrared spectra in the principal (OH)-stretching region for synthetic (OH)-excess amphibole (modified from Cámara et al. 2004)

regard to the crystal chemistry of the amphibole-supergroup minerals. Until fairly recently, it was assumed that (OH + F + Cl) = 2 apfu in amphiboles (with the exception of kaersutitic compositions). However, more recent work has shown that (OH + F + Cl) can be much less that 2 apfu in many compositions, and ideally anhydrous compositions with O ~24 apfu are now known. The possible incorporation of H^+ in excess of that required by (OH + F + Cl) = 2 apfu would broaden the flexibility of amphibole chemical compositions even further.

13.3.4 Quantum Tunnelling

Beryl, ideally $Be_3Al_2Si_6O_{18}$, may contain (H_2O) in the channels parallel to the **c**-axis. Infrared spectra (Wood and Nassau 1968) show two types of (H_2O) in beryl: type I with the H–H vector parallel to the **c**-axis and type II with the H–H vector perpendicular to the **c**-axis. Hawthorne and Černý (1977) showed that type I (H_2O) is non-bonded and type II (H_2O) is bonded to alkali metals that also lie within the channel, and assumed that type I (H_2O) is statically disordered over six possible orientations within the channel. Recent DFT calculations (Kolesnikov et al. 2016) showed that the potential barrier for rotation of (H_2O) around the **c**-axis is about 176 meV in accord with a model of static disorder. However, inelastic neutron-scattering spectra indicate extensive tunnelling of protons between the six symmetrically equivalent H positions within the channel and coherent delocalization of the protons that constitute a "new state" of the (H_2O) group (Kolesnikov et al. 2016). Examination of type I beryl as a function of pressure (Kolesnikov et al. 2019) showed that the vibrational and tunnelling modes of type I (H_2O) are very sensitive to the confining pressure. No tunnelling modes were observed for type II (H_2O) in either beryl or cordierite.

It will be interesting to see if such tunnelling effects extend to neutral H-bearing species that are itinerant at higher temperatures in zeolitic crystals.

13.3.5 $(OH)^-$–F^- Solid Solution: Constraints Imposed by Hydrogen Bonding

As $(OH)^-$ and F^- are isovalent, it might be thought that there should always be the possibility of solid solution between them. However, this is not the case. Where hydrogen bonding is relatively weak in a structure, possibly <0.20 *vu*, there is often extensive to complete solid solution of $(OH)^-$ and F^-. This situation is common in many key groups of rock-forming minerals, e.g., amphiboles (Hawthorne et al. 2012), micas (Rieder et al. 1999), in which the principal (OH)-stretching frequencies in the infrared are in the range 3500–3730 cm^{-1}. As noted above, this solid solution considerably increases the number of mineral species with substantial but non-essential $(OH)^-$. Where hydrogen bonding is stronger, the atomic arrangement cannot relax

sufficiently to accord with the valence-sum rule if F^- were to replace $(OH)^-$, and hence such solid solution does not happen, as is the case for the brackebuschite-supergroup minerals (see below).

Coupled hydrogen-bonding may lead to unusual constraints on solid solution of $(OH)^-$ and F^-. Consider the structure of hambergite, $Be_2(BO_3)(OH,F)$. There is no F-dominant species recognized by IMA-CMMNC and $F^- \rightarrow (OH)^-$ replacement reaches a maximum of 48% (Burns et al. 1995). Moreover, synthetic $Be_2(BO_3)F$ has a completely different structure (Baidina et al. 1978). In the F-free (F_0) composition (Fig. 13.11a), symmetrically equivalent $(OH)^-$ ions form a staggered hydrogen-bonded chain that extends in the **c**-direction. For the F_{50} composition, $(OH)^-$ and F^- alternate along the chain, and there are two possible hydrogen-bonding arrangements: (1) each H^+ ion may form a bifurcated hydrogen bond to the two adjacent F^- ions (Fig. 13.11b); (2) each H^+ ion may form a single hydrogen bond to the adjacent F^- ion (Fig. 13.11c). Whichever arrangement occurs for the F_{50} composition, it is apparent that F^- substitution for $(OH)^-$ cannot go beyond 50%. Such constraints on partial solid-solution of F^- and $(OH)^-$ are not uncommon in minerals.

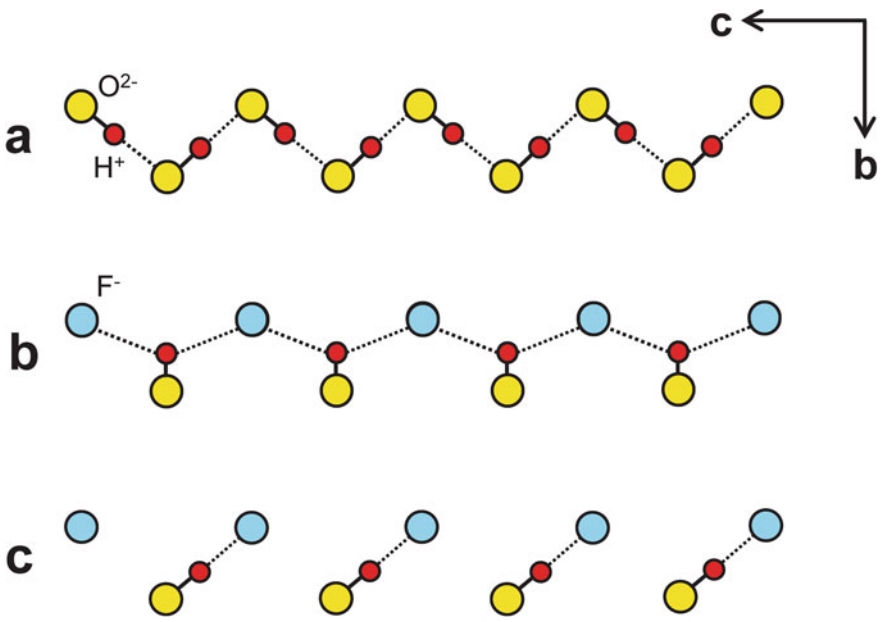

Fig. 13.11 Possible local F^-–OH^- arrangements along the hydrogen-bonded strips in hambergite. **a** All sites are occupied by OH^-; **b** one half the sites are occupied by F^- and the H^- ion forms a bifurcated hydrogen bond with adjacent F^- ions; **c** one half the sites are occupied by F^- with the occurrence of hydrogen-bonded O^{2-}–H^+…F^- pairs. Blue circles: F^- ions. Modified after Burns et al. (1995)

13.3.6 Trace H in Minerals

Wilkins and Sabine (1973) first showed that many nominally anhydrous silicate minerals contain trace levels of H^+ as $(OH)^-$ and proposed that this $(OH)^-$ is associated with some kind of defect or defects. Much subsequent effort was spent on developing accurate calibrations necessary to achieve quantitative chemical analysis of trace amounts of H. Bell and Rossman (1992) reported H contents on a cross-section of nominally anhydrous mantle and crustal minerals and addressed the issue of how much of the Earth's H is resident in the mantle. Subsequent estimates of the amount of H (expressed as H_2O) in the mantle have ranged from one to seven times the amount of H_2O in the oceans of Earth (Peslier et al. 2017).

13.4 Binary Structure Representation

A *structural unit* is defined as the strongly bonded part of a crystal structure and generally consists of oxyanions (e.g., $(SO_4)^{2-}$, $(SiO_4)^{4-}$) and trivalent and divalent cations in [5]- and [6]-coordination. An *interstitial complex* is defined as the weakly bonded part of a structure and generally consists of monovalent and divalent cations, (H_2O) and $(OH)^-$. This division of a structure into two constituent parts is illustrated in Fig. 13.12 for botryogen: $Mg_2(H_2O)_{10}[Fe^{3+}{}_2(SO_4)_4(H_2O)_2]_2$ (Majzlan et al. 2016).

On the one hand, these definitions give no indication of the strength of a bond for the constituent atoms to be considered as part of the structural unit. On the other hand, the definitions provide a degree of flexibility as the division between bonds where the cation belongs to the structural unit and bonds where the cation belongs to the interstitial species can depend on the relative distribution of bond valences and the topology of the bond network. This division is commonly taken at 0.30 *vu*, somewhat less than the Lewis acidities of the common [6]-coordinated divalent cations (Mg^{2+}, Fe^{2+}, Mn^{2+}, etc.; Gagné and Hawthorne 2017) and greater than the Lewis acidities of the common large divalent and monovalent cations (Na^+, K^+, Ca^{2+}, etc.). This division has the advantage that the strengths of $H^+ \ldots O^{2-}$ bonds in aqueous solution are similar to the strengths of bonds involving interstitial cations, and one can understand chemical reactions involving minerals exposed to aqueous solutions of varying pH as it is these weak interactions that control structure stability. Thus the *binary representation* of complex structure gives a simple but quantitative model of even the most complicated mineral, and provides insight into the weak interactions that control the stability of its structure.

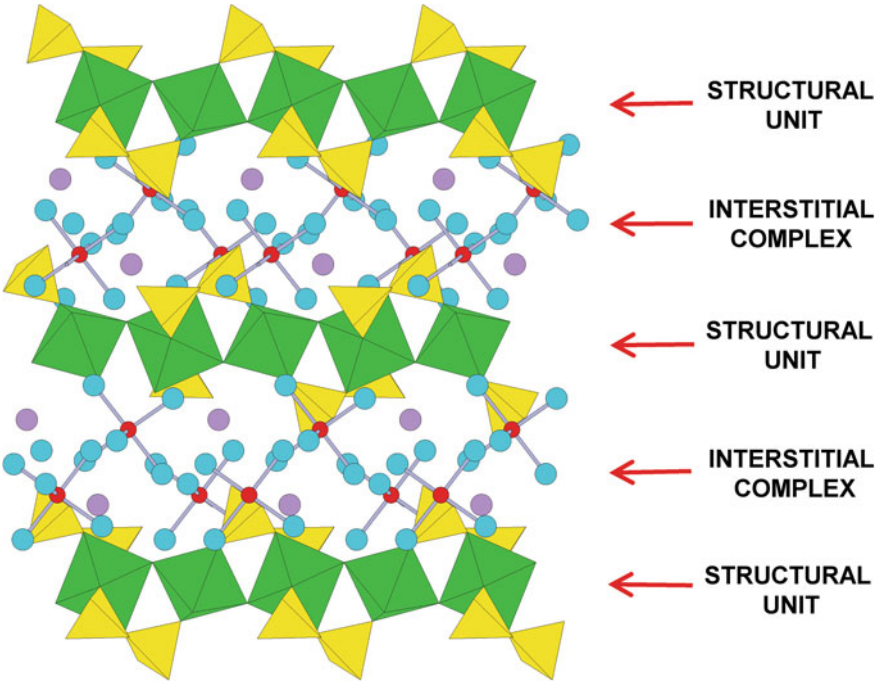

Fig. 13.12 The crystal structure of botryogen, $Mg_2(H_2O)_{12}[Fe^{3+}{}_2(SO_4)_4(OH)_2](H_2O)_2$, partitioned into two units, the strongly bonded structural unit (shown as colored polyhedra) and the weakly bonded interstitial complex (shown as individual atoms and chemical bonds). Yellow tetrahedra: (SO_4) groups; green octahedra: ($Fe^{3+}O_6$) octahedra; large blue circles: O^{2-} ions; small red circles: Mg^{2+} ions; mauve circles: (H_2O) groups linked only by hydrogen bonds; grey lines: Mg–O bonds. Modified after Hawthorne (2015)

13.5 The Effects of $(OH)^-$ and $(H_2O)^0$ on Dimensional Polymerization in Oxysalt Structures

The importance of $(OH)^-$ and $(H_2O)^0$ in oxysalt minerals arises from their very strong polarity and the fact that they have a net dipole moment. As is apparent from Fig. 13.3a, b, the oxygen side of each group functions as an anion, accepting a bond from a neighbouring cation, whereas the hydrogen side of each group functions as a cation, forming a bond with a neighbouring anion. The other ions in Fig. 13.3 have much higher symmetry with the result that although the bonds involving single H^+ ions are very asymmetric, this is not the case for the complexes themselves which act as polycations with Lewis acidities equal to the mean strength of their constituent hydrogen bonds.

For $(OH)^-$ and $(H_2O)^0$, the cation–O_{donor} bond(s) are commonly strong, ~0.8 and 0.4 *vu*, respectively, and form part of the structural unit, whereas on the Lewis-acid side of the group, the weaker (hydrogen) bonds do not form an integral part of the

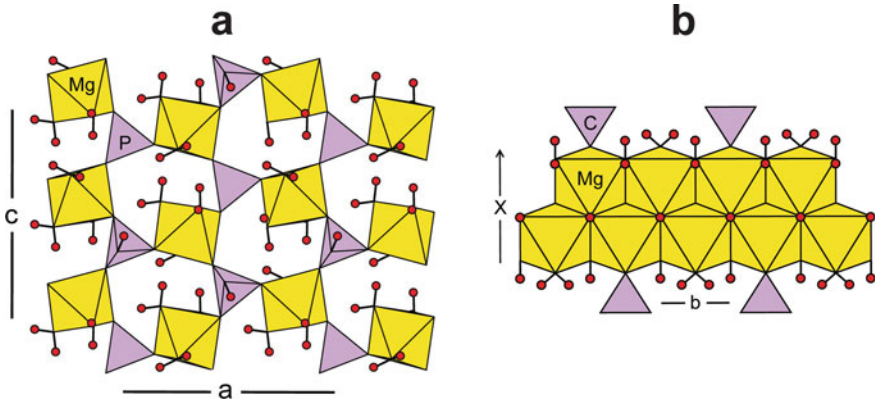

Fig. 13.13 **a** The crystal structure of newberyite, $Mg_3(PO_3OH)(H_2O)_3$, projected onto (010); **b** the crystal structure of artinite, $[Mg_2(CO_3)(OH)_2(H_2O)_3]$, projected onto (001); yellow octahedra: $(Mg\Phi_6)$ groups; lilac tetrahedra: $(P\Phi_4)$ groups; lilac triangles: (CO_3) groups. Modified after Hawthorne (2015)

structural unit unless they bond to an anion of the structural unit. Where the H^+ ion bonds to an interstitial anion, the resultant hydrogen bond is not part of the structural unit and the polymerization of the polyhedra of the structural unit is limited or terminated. Thus the speciation of H^+ and its position in the structural unit are major factors in controlling the dimension of polymerization of the coordination polyhedra in minerals (Hawthorne 1992).

Newberyite, $Mg_3(PO_3OH)(H_2O)_3$ (Sutor 1967), contains $(Mg\Phi_6)$ octahedra that link to $(P\Phi_4)$ tetrahedra to form a sheet parallel to **ac** with each tetrahedron sharing three vertices with adjacent octahedra (Fig. 13.13a). This arrangement leaves three octahedron vertices and one tetrahedron vertex that could potentially link to other strongly bonded polyhedra adjacent in the **b** direction to form a framework structure. A H^+ ion is attached to the free O^{2-} anion of the $(P\Phi_4)$ tetrahedron to form an acid phosphate group: $(PO_3OH)^{2-}$. The bond-valence incident at the O_{donor} ion is ~2 *vu* and prevents the constituent O^{2-} ion being part of another adjacent tetrahedron or octahedron. Similarly, H^+ ions attach to the free O^{2-} anions of the $(Mg\Phi_6)$ octahedron to form an $(MgO_3(H_2O)_3)^{4-}$ group. The bond-valence incident at each of the O_{donor} ions of the (H_2O) groups is ~2 *vu* and prevents them from being part of another tetrahedron or octahedron. Thus the presence of H^+ in newberyite prevents all linkage between the individual layers of tetrahedra and octahedra parallel to **ac**, and newberyite is a mixed tetrahedron-octahedron sheet structure in the structure hierarchy of the phosphate minerals (Huminicki and Hawthorne 2002).

The arrangement of the $(OH)^-$ and (H_2O) groups in newberyite prevents any linkage between adjacent layers of linked octahedra and tetrahedra. However, $(OH)^-$ and (H_2O) can allow linkage of a structural unit in some directions and prevent such linkage in other directions, depending on the local details of their stereochemistry. Artinite, $[Mg_2(CO_3)(OH)_2(H_2O)_3]$ (Akao and Iwai 1978) has a ribbon

of edge-sharing ($MgΦ_6$) octahedra decorated by (CO_3) triangles (Fig. 13.13b). The anions down the middle of the ribbon link to three Mg^{2+} which provide them with $0.36 \times 3 = 1.08$ *vu*, and are donor anions to their associated H^+ ions which weakly hydrogen-bond to a neighboring ribbon. Thus the $(OH)^-$ group prevents linkage of the structural unit in the **c**-direction but allows linkage in the **a**- and **b**-directions. The three anions along the margin of the ribbon bond to Mg^{2+}, $Mg^{2+}{}_2$ and $Mg^{2+} + C^{4+}$, with incident bond-valence values of ~0.3, 0.6 and 1.7 *vu*, corresponding to (H_2O), (H_2O) and O^{2-}, respectively. The first (H_2O) group prevents additional polymerization of the structural unit in all three directions, and the second (H_2O) group allows polymerization in the **b**-direction but prevents polymerization in the **a**- and **c**-directions.

Hydrogen as (OH) and (H_2O) can control the dimensional polymerization of a structural unit, limiting it in one or more directions. This is the principal mechanism that produces the wide structural diversity in oxygen-based minerals. Moreover, the distribution of H throughout the Earth, together with the anharmonic nature of the hydrogen bond and its response to variations in pressure, is a major factor in accounting for the systematic distribution of mineral species from the core to the surface of the Earth (Hawthorne 2015).

13.6 The Valence-Matching Principle and the Role of (H_2O)

Above, the valence-matching principle was stated as follows: Stable structures will form where the Lewis-acid strength of the cation closely matches the Lewis-base strength of the anion. What was not stated is that the valence-matching principle is the most important and powerful idea in bond-valence theory (Hawthorne 2012): it allows us to test whether a structure arrangement can exist or not, which moves us from *a posteriore* analysis to *a priori* analysis. I will consider two simple examples from Hawthorne (1994) to illustrate this principle.

Consider the composition Na_2SO_4. The Lewis basicity of the (SO_4) group is 0.13 *vu*. (Table 13.1) and the Lewis acidity of Na is 0.17 *vu* (Gagné and Hawthorne 2017). The Lewis basicity of the anion approximately matches the Lewis acidity of the cation, the valence-matching principle is satisfied, and thenardite, Na_2SO_4, is stable. Consider the composition Na_4SiO_4. The Lewis basicity of the (SiO_4) group is 0.33 *vu* (Table 13.1) and the Lewis acidity of Na is 0.17 *vu.* The Lewis basicity of the anion does not match the Lewis acidity of the cation, the valence-matching principle is not satisfied, and Na_4SiO_4 is not a mineral (or stable structure).

13.6.1 The Principle of Correspondence of Lewis Acidity-Basicity

In the examples of the valence-matching principle given above, the structural unit is a simple oxyanion, $(SO_4)^{2-}$ and $(SiO_4)^{4-}$, and the interstitial complex is a single cation, Na^+, and their interaction involves individual atom–atom interactions. This approach is not practical for minerals with a structural unit and an interstitial complex that both contain several different types of ions, e.g., metavoltine, $K_2Na_6Fe^{2+}Fe^{3+}{}_6O_2(SO_4)_{12}{\cdot}18H_2O$. Hawthorne (1997) showed that bond-valence theory is also valid as a mean-field approach, suggesting that we consider the structural unit as a very complicated oxyanion (or oxycation) and the interstitial complex as a complicated oxycation (or oxyanion). This approach allows us to define an aggregate Lewis basicity for the structural unit and an aggregate Lewis acidity for the interstitial complex, and the valence-matching principle may be generalized to the *principle of correspondence of Lewis acidity-basicity* (Hawthorne and Schindler 2008): *Stable structures will form where the Lewis-acid strength of the interstitial complex closely matches the Lewis-base strength of the structural unit.* Using this principle, we may examine the mean-field (average) interaction between the structural unit and the interstitial complex, an interaction in which the H^+ ion commonly plays a major role in promoting a more stable linkage between the two components of the structure (Schindler and Hawthorne 2001, 2004, 2008; Schindler et al. 2006).

13.6.2 (H_2O) as a Moderator of Bond Valence

As noted above, the H^+ ion usually has a very asymmetric coordination. As a result, $(OH)^-$ and $(H_2O)^0$ groups are very polar: the O^{2-} side of the group acts like an anion, whereas the H^+ side of the group acts as a cation with a (weak) hydrogen bond to any neighbouring anion.

(H_2O) bonded to one cation: Consider a cation, *M*, bonded to an anion, *S*, with a bond valence of v *vu* (Fig. 13.14a), and a cation, *M*, bonded to an (H_2O) group, each H^+ ion of which hydrogen-bonds to an anion, *S* (Fig. 13.14b). In Fig. 13.14a, S receives a bond valence of v *vu*; in Fig. 13.14b, S receives a bond valence of v/2 *vu*. The (H_2O) group bonded to a single *M* cation splits the *M*–O bond into two bonds of (on average) half the bond valence, *v*/2 *vu*, in effect acting as a *bond-valence transformer*: thus this type of (H_2O) is designated *transformer* (H_2O).

(H_2O) bonded to two cations: Consider two cations, *M*, bonded to an (H_2O) group, each H^+ ion of which hydrogen-bonds to an anion, *S* (Fig. 13.14c); each *S* receives a bond valence of v *vu*, the same bond valence as where it is bonded directly to one *M* cation (Fig. 13.14a). Here, (H_2O) does not act as a bond-valence transformer, and hence is denoted *non-transformer* (H_2O). Note that where the donor O^{2-} ion also accepts two hydrogen bonds, it is also part of a *non-transformer* (H_2O) group (Fig. 13.14d).

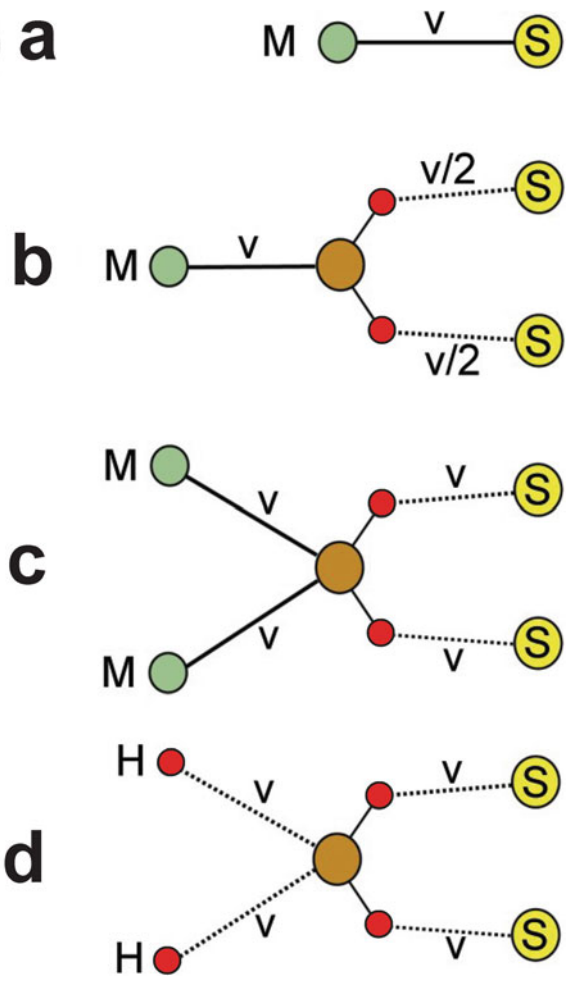

Fig. 13.14 Bond-valence structure around (H_2O) as a function of local bond-topology: **a** a cation M bonds to an anion, S, with bond valence v *vu*; **b** M bonds to O_{donor} of an (H_2O) group with bond valence v *vu*; the H^+ ions hydrogen bond to S with bond valence v/2 *vu*; **c** two cations bonded to O_{donor} of an (H_2O) group with bond valence v *vu* and the H^+ ions hydrogen bond to S with bond valence v *vu*; **d** two H^+ ions hydrogen bond to O_{donor} of an (H_2O) group and the H^+ ions of the (H_2O) group hydrogen bond to S with bond valence v *vu*. Green circle: M cation; brown circle: O_{donor}; yellow circle: $O_{acceptor}$. Modified after Hawthorne (2012, 2015)

In the arrangements of Fig. 13.14, the $O_{acceptor}$ anions are tacitly assumed to be simple anions. However, there is an additional possibility: the $O_{acceptor}$ anions can be part of an (H_2O) group of the interstitial complex; this arrangement is shown in Fig. 13.15 in which the bond valences to the final $O_{acceptor}$ anions S are one quarter of the original bond-valence of the cation M involved in the arrangement. This double-transformer effect greatly expands the range and Lewis acidity of the cations that can be incorporated into the interstitial complex as shown above.

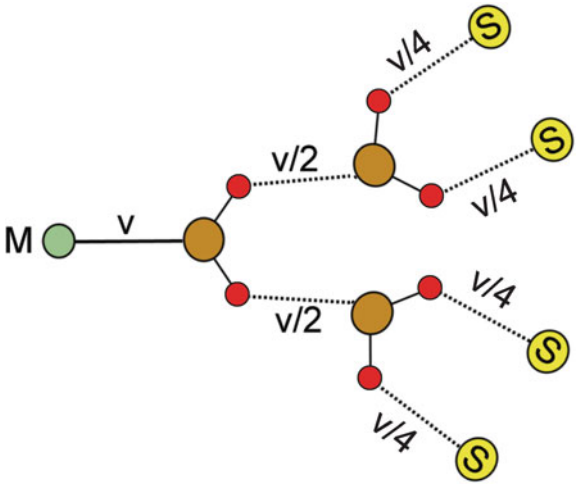

Fig. 13.15 A cation M bonds to O_{donor} of an (H_2O) group with bond valence v *vu*, the H^+ ions of the (H_2O) group hydrogen bond to O_{donor} of two interstitial (H_2O) groups with bond valence v/2 *vu*, and the H^+ ions of each interstitial (H_2O) group hydrogen bond to $O_{acceptor}$ anions with bond valence v/4 *vu*

13.6.3 An Example: The Pascoite-Family Decavanadate Minerals

The decavanadate isopolyanion, ideally $[V_{10}O_{28}]^{6-}$ (Fig. 13.16), is a constituent of the pascoite-family vanadate minerals (Kampf et al. 2021) and their synthetic analogues, and there are protonated, $[H_xV_{10}O_{28}]^{(6-x)-}$, and mixed-valence, $[(V^{4+}{}_xV^{5+}{}_{10-x})O_{28}]^{(6+x)-}$, varieties (Table 13.4). They occur as low-temperature phases associated with the roll-front U deposits of the Colorado Plateau, and their synthetic analogues have wide application in industry as coatings, gas sorbents, sensors, dyes, capacitors and cation exchangers, and in medicine as anti-tumor agents, antiviral agents, cancer antagonists, and in the treatment of Alzheimer's disease. The structural units of these minerals show a limited range of Lewis basicity (0.054–0.154 *vu*) but the interstitial complexes show a wide range in chemical composition, and the question arises as to how these compositions accord with the principle of correspondence of Lewis acidity-basicity (Hawthorne et al. 2022). Figure 13.17 shows the variation in Lewis acidity and mean coordination number for all cations of the Periodic Table with Lewis acidities <0.80 *vu*, with the range of Lewis basicity of the decavanadate polyions shown as green circles and the Lewis basicity of individual decavanadate O^{2-} anions shown as black circles. According to the valence-matching principle, the only simple cations that can bond to the decavanadate ions are Na^+ to Cs^+, and it is notable that synthetic decavanadates of industrial interest commonly involve Cs^+ as an interstitial cation. Inspection of Table 13.4 shows that the pascoite-family minerals contain univalent, divalent and trivalent cations as interstitial components, and it is transformer (H_2O) that allows this to occur. Figure 13.15 shows how polycations bonded to two linked (H_2O) groups have their bond valences reduced by a factor 0.25. We may write these polycations as $M^{n+}(H_2O)_{0-6}$ and $M^{n+}(H_2O)_6(H_2O)_{0-12}$ with Lewis acidities varying from 0.50 to 0.13 *vu* for M^{3+} and from 0.33 to 0.08

vu for M^{2+}. As shown in Fig. 13.18, the Lewis acidities of these polycations are reduced such that they may now bond to the decavanadate polyanion in accord with the valence-matching principle. It is interesting to examine the polycations involving Al^{3+} in these structures. The series of polycations in Fig. 13.19a–c may be written as the chain $[Al_n(OH)_{2(n-1)}(H_2O)_{2(n+2)}]^{(n+2)+}$ which has a Lewis acidity of 0.25 *vu*, independent of the value of n, the number of octahedra in the chain, which adds an extra degree of flexibility in linking to the polyanion in the presence of additional simple interstitial cations. As shown in Fig. 13.19d, e, these polycations can become as complicated as their coexisting polyanions. As is apparent by comparison of Table 13.4 and Fig. 13.17, none of these minerals could exist without the moderating effect of transformer (H_2O).

Table 13.4 The minerals of the pascoite family

Mineral species	Ideal formula
Decavanadaites:	
Ammoniolasalite	$(NH_4)_2Mg_2[V_{10}O_{28}]\cdot 20H_2O$
Burroite	$(NH_4)_2Ca_2[V_{10}O_{28}]\cdot 15H_2O$
Gunterite	$Na_2Ca_2[V_{10}O_{28}]\cdot 22H_2O$
Huemulite	$Na_4Mg[V_{10}O_{28}]\cdot 24H_2O$
Hughesite	$Na_3Al[V_{10}O_{28}]\cdot 22H_2O$
Hummerite	$K_2Mg_2[V_{10}O_{28}]\cdot 16H_2O$
Hydropascoite	$Ca_3[V_{10}O_{28}]\cdot 24H_2O$
Kokinosite	$Na_2Ca_2[V_{10}O_{28}]\cdot 24H_2O$
Lasalite	$Na_2Mg_2[V_{10}O_{28}]\cdot 20H_2O$
Magnesiopascoite	$Ca_2Mg[V_{10}O_{28}]\cdot 16H_2O$
Okieite	$Mg_3[V_{10}O_{28}]\cdot 28H_2O$
Pascoite	$Ca_3[V_{10}O_{28}]\cdot 17H_2O$
Postite	$MgAl_2(OH)_2[V_{10}O_{28}]\cdot 27H_2O$
Protocaseyite	$[Al_4(OH)_6(H_2O)_{12}][V_{10}O_{28}]\cdot 8H_2O$
Rakovanite	$(NH_4)_3Na_3[V_{10}O_{28}]\cdot 12H_2O$
Schindlerite	$(NH_4)_4Na_2[V_{10}O_{28}]\cdot 10H_2O$
Wernerbaurite	$(NH_4)_2Ca_2[V_{10}O_{28}]\cdot 16H_2O$
Mixed-valence and protonated mixed-valence decavandaites:	
Bluestreakite	$K_4Mg_2[(V^{4+}{}_2V^{5+}{}_8)O_{28}]\cdot 14H_2O$
Caseyite	$[(V^{5+}O_2)Al_{7.5}(OH)_{15}(H_2O)_{13}]_2[H_2V^{4+}V^{5+}{}_9O_{28}][V^{5+}{}_{10}O_{28}]_2\cdot 90H_2O$
Nashite	$Na_3Ca_2[(V^{4+}V^{5+}{}_9)O_{28}]\cdot 24H_2O$
Trebiskyite	$Na_3Mg_2[(Ti^{4+}V_9)O_{28}]\cdot 22H_2O$

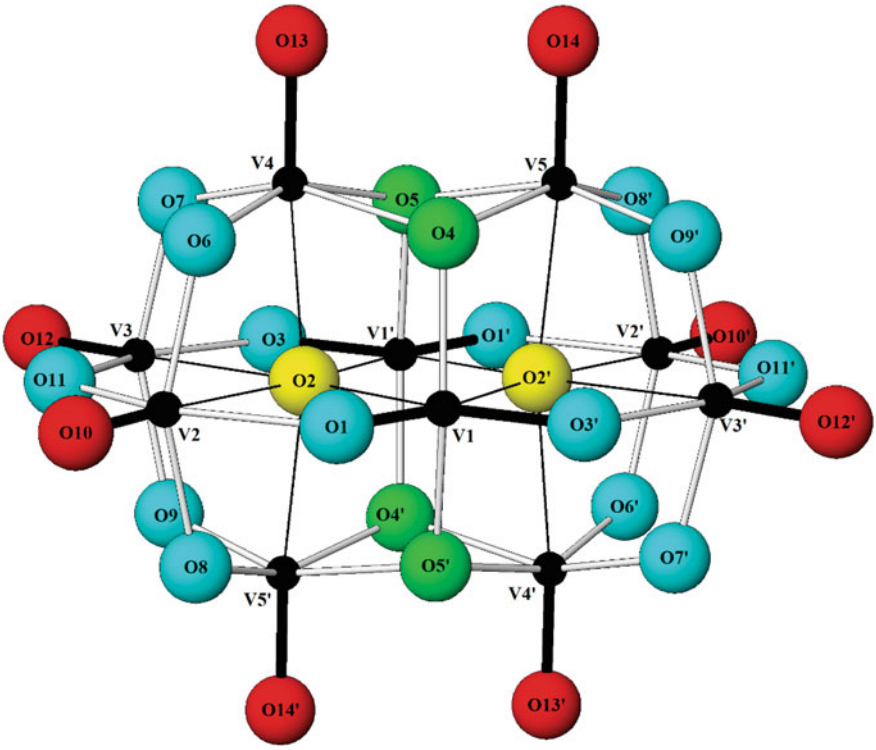

Fig. 13.16 The $[V_{10}O_{28}]^{6-}$ decavanadate polyanion. Small black circles: V^{5+} ions; red circles: [1]-coordinated O atoms; blue circles: [2]-coordinated O atoms; green circles: [3]-coordinated O atoms; yellow circles: [6]-coordinated O atoms; thick black line: $V–O_{vanadyl}$ bond; thin black line: $V–O_{trans}$ bond; gray shaded line: $V–O_{equatorial}$ bond. From Hawthorne et al. (2022)

13.7 Multi-scale Processes from Small-Scale Mechanisms

Although H is the smallest element, and the mechanisms by which it is incorporated into mineral structures are on the scale of Ångstroms, the effects of many of these mechanisms occur on scales from microns to meters to thousands of kilometres. As Earth scientists, we are aware of many of these effects and accept them without paying too much attention to the critical role played by hydrogen. Lovelock and Margulis (1973) emphasize the importance of water to the Gaia hypothesis in the second sentence of their abstract: "The geological record reads that liquid water was always present and that the pH was never far from neutral". The principal thrust of their argument involves the atmosphere and the biosphere, but the solid Earth and the oceans are also involved in this synergy, particularly when considered from the point of view of H rather than just the liquid and vapour phases of H_2O. Here I will just mention a few of the well-known large-scale processes, and discuss in more

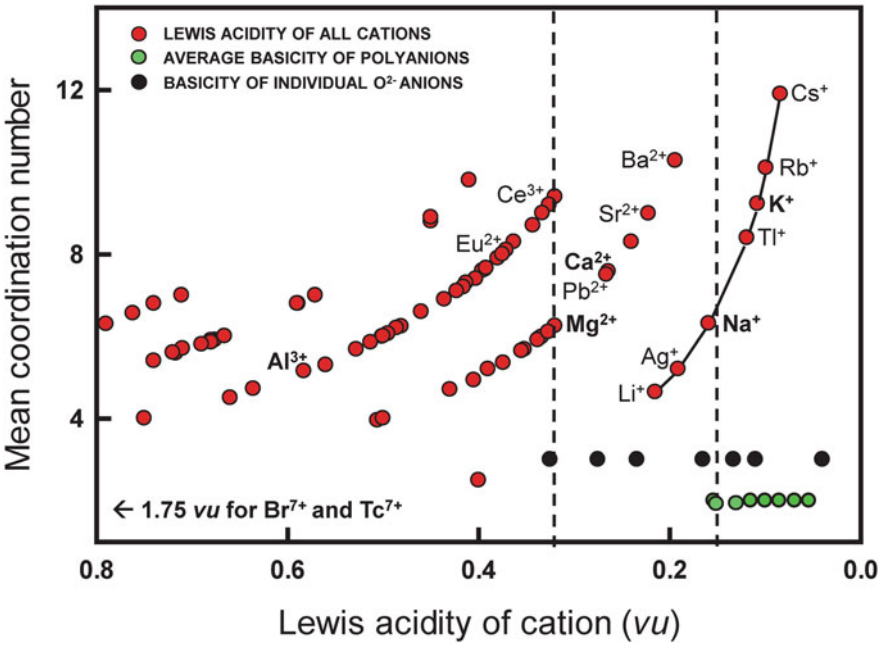

Fig. 13.17 Mean observed coordination number for 91 cations as a function of their Lewis acidity (red circles). Green circles: Lewis basicities of the decavanadate structural units; black circles: bond-valence deficiencies of various O^{2-} ions of the vanadate unit. The black dashed lines denote the maximum value of the green circles and black circles, respectively. Modified from Hawthorne et al. (2022)

detail the roles of H^+ in two of the more recently described medium- and large-scale processes in which the details of the atom-scale mechanisms have been proposed.

13.7.1 Medium-Scale Processes: Relative Humidity as a Driver of Structural Change

The direct interaction of minerals with H_2O in ambient air has long been recognized as a significant process, particularly by mineral collectors and museum curators. Perhaps most widely known example is the oxidation of marcasite and some forms of pyrite to form sulfuric acid plus various Fe^{2+}-sulfates: e.g., $Fe^{2+}(SO_4)(H_2O)_n$ from szomolnokite (n = 1) to melanterite (n = 7) and a wide variety of mixed (Fe^{2+}–Fe^{3+})-sulfates and Fe^{3+}-sulfates, a process widely known as *pyrite decay*. Although such solid–vapor reactions may play a role in acid-mine drainage, it is generally subsidiary to aqueous reactions.

The recent description of the reversible hydration ↔ dehydration of metatamboite-tamboite is particularly interesting as it proposes a mechanism of hydration

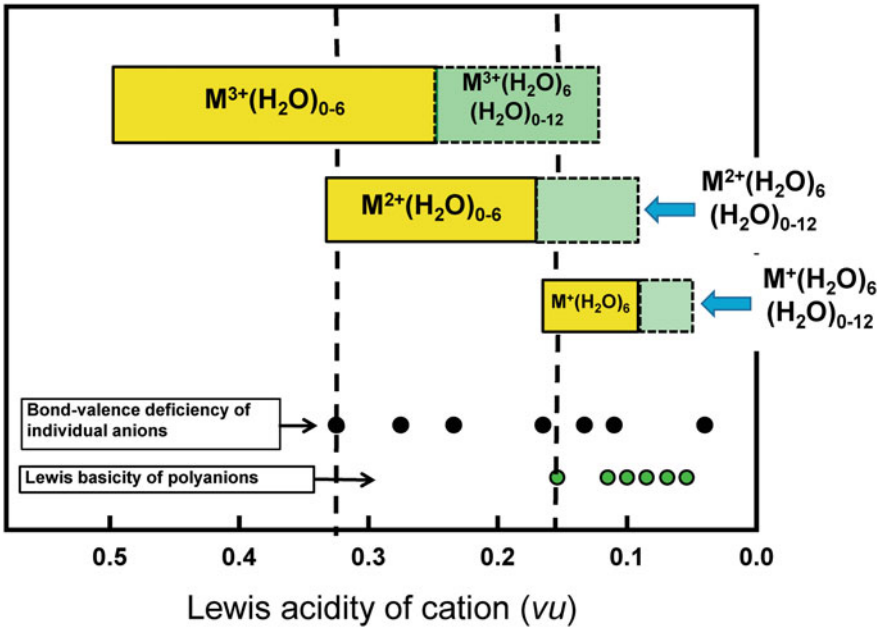

Fig. 13.18 Ranges in Lewis acidity of interstitial polycations with one layer of coordinating transformer (H_2O) groups (yellow boxes) and with two layers of coordinating transformer (H_2O) groups (green boxes); legend as in Fig. 13.17. Modified from Hawthorne et al. (2022)

that is related to the structure of atmospheric H_2O (Cooper et al. 2019). These minerals have the following general formula: $Fe^{3+}{}_3(SO_4)(Te^{4+}O_3)_3(Te^{4+}O(OH)_2)(OH)(H_2O)_x\{H_2O\}_y$ with x = 3, y = 0 for metatamboite and x = 3, y = 2 for tamboite. The structures contain topologically identical ferric-iron-sulfate-tellurite-hydrate slabs parallel to (011). In metatamboite, these slabs are linked by hydrogen bonds bridging adjacent slabs (Fig. 13.20a, hydrogen bonds not shown in this figure to emphasize the space between each slab). In tamboite (Fig. 13.20b), there are an additional four (H_2O) groups forming an $\{(H_2O)_4\}$ cluster with the internal and external hydrogen bonds shown by red and black dotted lines, respectively. (H_2O) enters and leaves the structures with variation in ambient humidity, and this change is reversible, whereas exposure to a desiccant results in irreversible dehydration and melding of the slabs into a framework structure.

The four (H_2O) groups form a homodromic hydrogen-bonded cyclic tetramer (Fig. 13.20a) in the interstices between the slabs in tamboite (Fig. 13.20b), denoted as $\{(H_2O)_4\}$, the interstitial complex in tamboite. There are two low-energy square-planar cyclic tetramers with homodromic hydrogen bonding: the S_4 tetramer in which the out-of-plane H^+ ions are in a *udud* (up-down-up-down) arrangement relative to the plane of the square, and the C_i tetramer in which the out-of-plane H^+ ions are in the *uudd* arrangement. Both tetramers are major constituents of the Earth's lower-atmosphere under humid conditions, with approximate concentrations

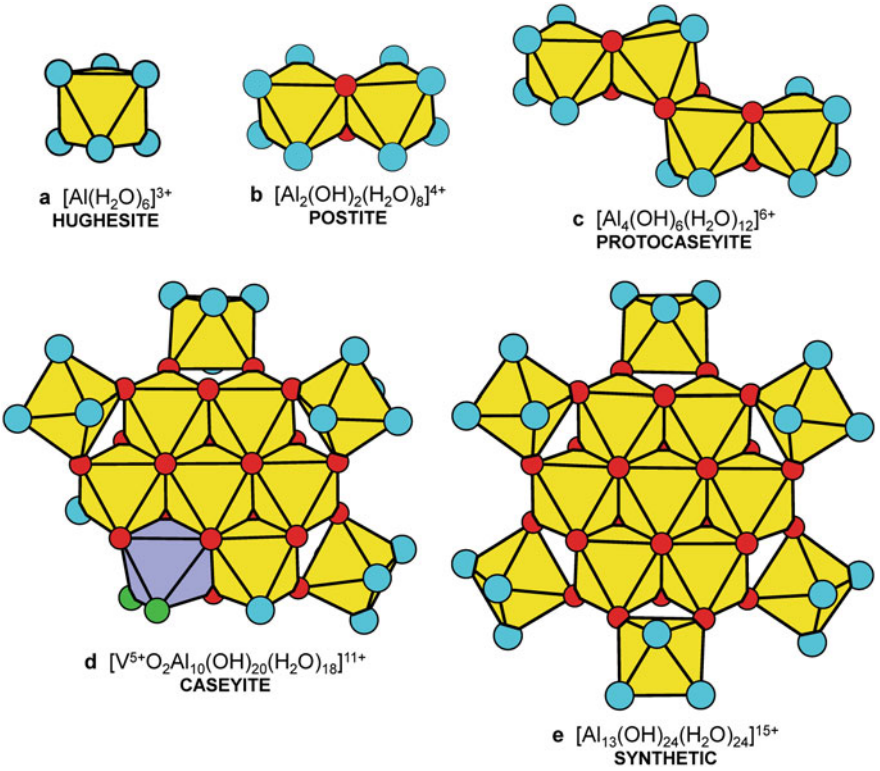

Fig. 13.19 Polycations involving Al^{3+} in decavanadate minerals: **a** the monomer $[Al(H_2O)_6]^{3+}$ in hughesite; various flatimers in minerals: **b** postite; **c** protocaseyite; **d** caseyite; **e** synthetic $[Al_{13}(OH)_{24}(H_2O)_{24}]Cl_{15}(H_2O)_{13}$. Blue circles: (H_2O); red circles: $(OH)^-$; green circles: O^{2-} ions. Modified from Hawthorne et al. (2022)

of 10^{11} clusters/cm^3). The absorption of $(H_2O)_4$ clusters is shown conceptually in Fig. 13.20a, where planar atmospheric $(H_2O)_4$ clusters enter (and exit) the interstitial space between the structural units, accompanied by shear between adjacent slabs as shown by the red arrow in Fig. 13.20a. We do not know if the mechanism suggested actually occurs, but it is of interest to identify which other atmospheric $(H_2O)_n$ clusters may be active in hydration-dehydration reactions in other minerals.

13.7.2 Large-Scale Processes from Small-Scale Mechanisms

From a geochemical perspective, H_2O has many unusual properties that are critical to its roles on Earth. H_2O is the only common substance to exist as solid, liquid and vapour under surface conditions on Earth. As a constituent of H_2O, H with its small size, mobility and wide range of possible bond-valence can exchange easily

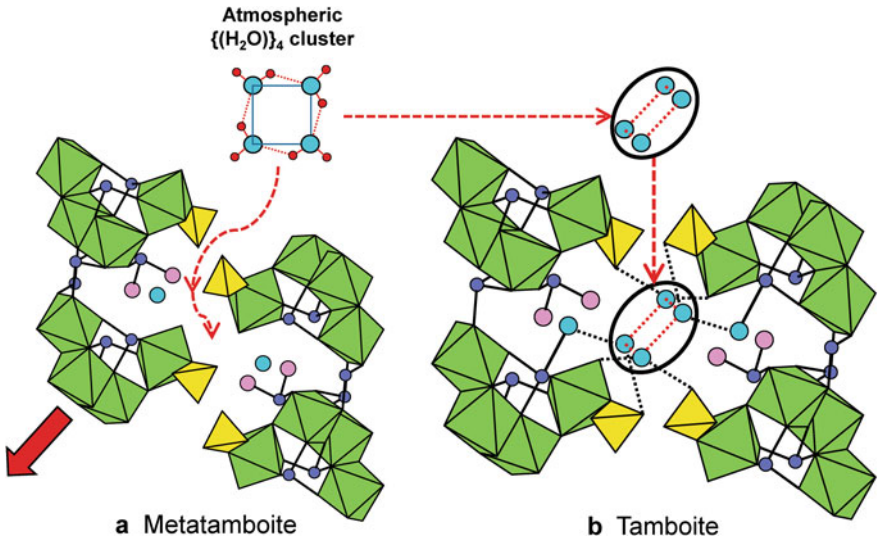

Fig. 13.20 Parts of the adjacent structural slabs in the crystal structures of **a** metatamboite and **b** tamboite; the H atoms and the interslab hydrogen bonds are omitted in (**a**) and (**b**) for clarity. The compositional difference between (**a**) and (**b**) is the square cluster of (H_2O) groups in (**b**) marked by the black ellipse. In (**a**), the solid red arrow indicates the direction of movement of the left slab when atmospheric $\{(H_2O)_4\}$ is introduced into the structure (along the dashed red arrow) between the two slabs. Green octahedra: ($Fe\Phi_6$); yellow tetrahedra: (SO_4); dark-blue circles: Te^{6+}; pink circles: $(OH)^-$; pale-blue circles: (H_2O); red dotted lines: O_{donor}–H^+…$O_{acceptor}$ linkages within the $\{(H_2O)_4\}$ cluster; black dotted lines: O_{donor}–H^+…$O_{acceptor}$ linkages external to the $\{(H_2O)_4\}$ cluster. Modified from Cooper et al. (2019)

and rapidly between solid, liquid and vapour phases, making it the most pervasive element on Earth (sensu lato). For example, it is hydrogen bonds that give water its high surface tension, and it is this high surface tension that is essential to the existence of vascular plants (including trees), a large group of land plants containing lignified tissue through which water and nutrients are transported upward via surface tension between water and the internal surfaces of the plant.

The bicarbonate polyanion $(CO_2(OH))^-$ shows the profound effect of acid dissociation in Earth processes and the crystallization of minerals. $(CO_2(OH))^-$ is bounded by pK_a values of 6.4 and 10.3 and reaches its maximum concentration in aqueous solution at a pH of ~8.3; as a consequence, bicarbonate is the dominant form of dissolved inorganic C in sea water. Rainwater contains weak carbonic acid that reacts with surficial rocks to produce bicarbonate in freshwater which eventually finds its way to the sea. Bicarbonate has a Lewis basicity that matches extremely well with the pH of near-neutral water and thus bicarbonate remains in solution. High concentrations of bicarbonate and Ca^{2+} in solution will result in precipitation of calcium carbonate as the Lewis acidity of Ca^{2+} matches much better with $(CO_3)^{2-}$ than with $(CO_2(OH))^-$, and chemical sediments are dominated by limestones sensu lato.

13.7.2.1 Ice

H_2O is unlike most compounds in that the density of the solid (ice) is less than that of the liquid (water) which results in ice being one of the most (if not the most) important minerals on Earth. (1) In cold climates, ice forms on the surface of terrestrial water (lakes, rivers), insulating the underlying water and allowing aquatic life to survive the cold winters. (2) Sea level is controlled dominantly by the amount of (non-floating) ice, and climatic variations result in drastic changes in sea level with changes in terrestrial ice, resulting in major changes in glacial erosion, ice loading on the crust, and drastic changes in sea level.

13.7.2.2 Polarons and Mobile H^+: Anomalous Conductivity in Subduction Zones

There has been an enormous amount of work on oxidation-dehydroxylation mechanisms in amphiboles, particularly riebeckite (Della Ventura et al. 2018; Oberti et al. 2018) and the mechanism may be summarized as follows (Bernardini et al. 2022):

$$^{C}Fe^{2+} + {}^{W}(OH)^{-} \leftrightarrow {}^{C}Fe^{3+} + e^{-} + {}^{W}O^{2-} + H^{+} \rightarrow 1/4\,{}^{ext}O_2 \rightarrow {}^{C}Fe^{3+} + {}^{ext}e^{-} + {}^{W}O^{2-} + 1/2\,{}^{ext}H_2O$$

Oxidation of Fe^{2+}, primarily at the $M(1)$ site, couples to the release of an electron and disassociation of the bonded $(OH)^-$ anion to O^{2-} and H^+, and the electron and the H^+ ion migrate through the crystal, the latter to react with oxygen at the surface of the mineral and be released as H_2O in the presence of oxygen. High-temperature resonance Raman scattering shows the presence of thermally activated anisotropic small polarons caused by coupling of longitudinal optical (LO) polar phonons and conduction electrons arising from electron transitions in $^{[6]}Fe^{2+}$ and the accompanying strain associated with the reduction in size of the M octahedra caused by the oxidation of Fe^{2+} to Fe^{3+} (see overviews by Mihailova et al. 2021, 2022). The overall process begins with the onset of activation of small polarons (at temperature T' as denoted by Bernardini et al. 2022), continues to completion of polaron activation and H^+ delocalization (at T″), and concludes with the termination of dehydrogenation (T″'). The onset of itinerant small polarons and mobile H^+ (protons) greatly increases the electrical conductivity of the amphibole, and is accompanied by the delocalization of H^+ and its release as H_2O in the presence of external oxygen.

Anomalous high-conductivity layers and H_2O recycling are characteristic of subduction zones. Blueschists characteristically contain alkali amphiboles, particularly glaucophane, the Mg-dominant analogue of riebeckite. As described in detail by Bernardini et al. (2022), oceanic crust subducts beneath southwest Japan and enters the eclogite facies at a depth of ~50 km (Fig. 13.21a) and a low seismic-velocity layer extends to 60 km, the maximum depth of intraslab earthquakes. Oceanic crust subducting beneath north-eastern Japan enters the eclogite facies at a depth of 110 km

(Fig. 13.21b), the low-velocity layer extends to 150 km and intraslab earthquake activity to 200 km. The shaded regions in Fig. 13.21a show the P–T conditions for the subducting crust and the temperatures T′, for the onset of activation of small polarons and H^+ delocalization, T″ for the cessation of small polarons and H^+ delocalization, and T‴ for the termination of dehydrogenation. In the warm SW Japan subduction zone (Fig. 13.21b), shallow activation of small polarons and dehydrogenation are consistent with a shallow conductivity anomaly, shallow intraslab earthquakes, and sparse arc volcanism. In the cold NE Japan subduction zone (Fig. 13.21c), deep activation of small polaron conduction and dehydrogenation are consistent with a deep conductivity anomaly, deep intraslab earthquakes, and abundant arc volcanism.

The thermal structure of a subducting slab controls (1) the depth of activation of small polarons and H^+ delocalization, (2) the depth for the cessation of small

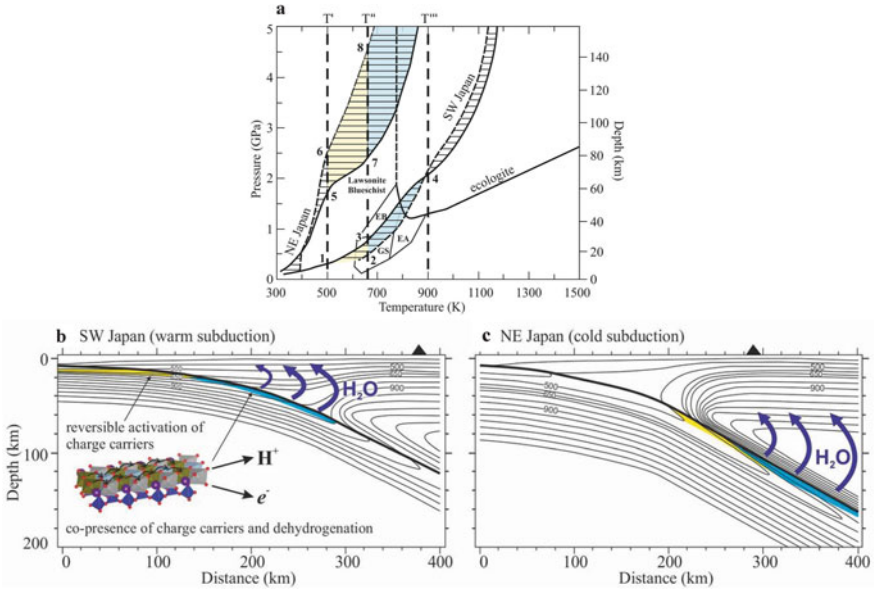

Fig. 13.21 Calculated PT conditions for oceanic crust subducted beneath SW and NE Japan; the stability for eclogite, lawsonite-blueschist, epidote blueschist (EB), epidote amphibolite (EA) and greenschist (GS) facies rocks are indicated. Contour interval: 100 K. Solid lines: top of subducting oceanic crust; dashed line: base of subducting oceanic crust. Under NE Japan, the top of the descending slab is colder than the base of the descending slab; the situation is reversed for the SW Japan. In this latter area, the temperature at the base and top of the slab are predicted to be equal at 65 km depth and reverse at greater depth. **b**, **c** Cross sections and calculated thermal structure for SW and NE Japan subduction zones. **a** The temperatures T′, T″, and T‴ mark the onset of polaron formation, completion of polaron activation and H^+ delocalization, and completion of amphibole dehydrogenation, respectively. The yellow areas denote the range of fully reversible activation of charge carriers, and the blue areas denote the presence of mobile polarons and itinerant H^+ with evolving Fe-oxidation and dehydrogenation. Blue arrows: aqueous fluids produced during dehydrogenation. Black triangles at the surface in (b) and (c) show the locations of the volcanic front. Figures assembled from Bernardini et al. (2022)

polarons and H^+ delocalization, and (3) the depth for the termination of dehydrogenation. Small polarons and delocalization of H^+ provide the atomic-scale mechanisms whose macroscopic-scale expression controls the presence of conductivity anomalies, affects H_2O recycling and the depth and strength of associated earthquakes and arc volcanism in subducting regimes.

13.8 Coda

(1) There are two features that distinguish H^+ from every other ion: it is the smallest element (Rahm et al. 2017), and it shows the greatest variation in the strength of its chemical bond to O^{2-}. Its small size means that it is by far the most mobile ion in a crystal, both with regard to speed of diffusion (e.g., Table 13.3) and capability of diffusion (it can pass through much smaller constrictions in a structure than any other ion). Variation in strength of its chemical bonds give H a diversity of roles in both solids and fluids that is not matched by any other element.

(2) H^+ is incorporated in crystals predominantly as polyions that may be Lewis bases, neutral complexes and Lewis acids: $(OH)^-$, $(CH_3)^-$, $(H_2O)^0$, $(NH_3)^0$, $(CH_4)^0$, $(H_3O)^+$, $(H_5O_2)^+$, $(NH_4)^+$, but also may occur as itinerant H^+.

(3) Bond-valence theory provides a very effective approach to understanding the structural and chemical diversity of oxide and oxysalt minerals. In particular, hydrogen has a pivotal role to play in matching the Lewis basicities of the structural units and the Lewis acidities of the interstitial complexes such that a wide diversity of minerals exists over a wide range of pH, Eh, T, P and activities of their various constituents.

(4) Although the critical features of H^+ (size, bonding characteristics) are at the Ångstrom level, their behaviour can provide the atomic-scale mechanism for processes whose macroscopic expression occurs on a global scale.

References

Akao M, Iwai S (1978) The hydrogen bonding of artinite. Acta Crystallogr B 33:3951–3953

Atencio D, Chukanov NV, Nestola F, Witzke T, Coutinho JMV, Zadov AE, Contreira Filho RR, Färber G (2012) Mejillonesite, a new acid sodium, magnesium phosphate mineral, from Mejillones, Antofagasta, Chile. Am Min 97:19–25

Baidina IA, Bakakin VV, Podberezskaya NV, Alekseev VI, Batsanova LR, Pavlyuchenko VS (1978) Crystal structure of beryllium fluoride borate. Zh Strukt Khim 19:125–129 (in Russian)

Bell DR, Rossman GR (1992) Water in Earth's mantle: the role of nominally anhydrous minerals. Science 255:1391–1397

Bernardini S, Della Ventura G, Schluter JJ, Mihailova B (2022) Electron-phonon coupling in amphiboles contributes to the anomalous conductivity in subduction zones. https://doi.org/10.21203/rs.3.rs-1696117/v1

Brown ID (1976) On the geometry of O-H...O hydrogen bonds. Acta Crystallogr A 32:24–31
Brown ID (1981) The bond-valence method: an empirical approach to chemical structure and bonding. In: O'Keeffe M, Navrotsky A (eds) Structure and Bonding in Crystals, vol 2. Academic Press, New York, pp 1–30
Brown ID (2002) The chemical bond in inorganic chemistry. Oxford University Press, U.K, The Bond Valence Model
Brown ID (2016) The chemical bond in inorganic chemistry. The Bond Valence Model. 2nd edition. Oxford University Press, U.K
Brown ID, Altermatt D (1985) Bond-valence parameters obtained from a systematic analysis of the Inorganic Crystal Structure Database. Acta Crystallogr B 41:244–247
Burns PC, Novák M, Hawthorne FC (1995) Fluorine-hydroxyl variation in hambergite: a crystal-structure study. Can Min 33:1205–1213
Cámara F, Oberti R, Della Ventura G, Welch MD, Maresch WV (2004) The crystal-structure of synthetic $NaNa_2Mg_5Si_8O_{21}(OH)_3$, a triclinic C-1 amphibole with a triple-cell and excess hydrogen. Am Min 89:1464–1473
Chukanov NV, Britvin SN, Möhn G, Pekov IV, Zubkova NV, Nestola F, Kasatkin AV, Dini M (2015) Shilovite, natural copper(II) tetrammine nitrate, a new mineral species. Min Mag 79:613–623
Cooper MA, Hawthorne FC, Abdu YA, Walford PC, Back ME (2019) Relative humidity as a driver of structural change in three new ferric-sulfate-tellurite hydrates: New minerals tamboite and metatamboite, and a lower-hydrate derivative, possibly involving direct uptake of atmospheric $\{H_2O\}_4$ clusters. Can Min 57:605–635
Della Ventura G, Mihailova B, Susta U, Guidi MC, Marcelli A, Schluter J, Oberti R (2018) The dynamics of Fe oxidation in riebeckite: a model for amphiboles. Am Min 103:1103–1111
Emsley J, Jones DJ, Lucas J (1981) Detecting and measuring strong hydrogen bonds: recent developments. Rev Inorg Chem 1981:105–140
Ferraris G, Franchini-Angela M (1972) Survey of the geometry and environment of water molecules in crystalline hydrates studied by neutron diffraction. Acta Crystallogr B 28:3572–3583
Ferraris G, lvaldi G (1984) X–OH and O–H...O bond lengths in protonated oxyanions. Acta Crystallogr B40:1–6
Gagné O, Hawthorne FC (2015) Comprehensive derivation of bond-valence parameters for ion pairs involving oxygen. Acta Crystallogr B 71:562–578
Gagné O, Hawthorne FC (2017) Empirical Lewis-acid strengths for 135 cations bonded to oxygen. Acta Crystallogr B 73:956–961
Gagné O, Hawthorne FC (2018) Bond-length distributions for ions bonded to oxygen: Results for the non-metals and discussion of lone-pair stereoactivity and the polymerization of PO_4. Acta Crystallogr B 74:79–96
Gagné O, Mercier PHJ, Hawthorne FC (2018) A priori bond-valence and bond-length calculations in rock-forming minerals. Acta Crystallogr B 74:470–482
Groat LA, Hawthorne FC, Ercit TS (1992a) The chemistry of vesuvianite. Can Min 30:19–48
Groat LA, Hawthorne FC, Ercit TS (1992b) The role of fluorine in vesuvianite: a crystal-structure study. Can Min 30:1065–1075
Groat LA, Hawthorne FC, Rossman GR, Ercit TS (1995) The infrared spectroscopy of vesuvianite in the OH region. Can Min 33:609–626
Hawthorne FC (1992) The role of OH and H_2O in oxide and oxysalt minerals. Z Kristallogr 201:183–206
Hawthorne FC (1994) Structural aspects of oxides and oxysalt crystals. Acta Crystallogr B 50:481–510
Hawthorne FC (1997) Short-range order in amphiboles: a bond-valence approach. Can Min 35:203–218
Hawthorne FC (2012) A bond-topological approach to theoretical mineralogy: crystal structure, chemical composition and chemical reactions. Phys Chem Min 39:841–874
Hawthorne FC (2014) The structure hierarchy hypothesis. Min Mag 78:957–1027

Hawthorne FC (2015) Toward theoretical mineralogy: a bond-topological approach. Am Min 100:696–713
Hawthorne FC, Černý P (1977) The alkali-metal positions in Cs–Li beryl. Can Min 15:414–421
Hawthorne FC, Schindler M (2008) Understanding the weakly bonded constituents in oxysalt minerals. Z Kristallogr 223:41–68
Hawthorne FC, Oberti R, Harlow GE, Maresch W, Martin RF, Schumacher JC, Welch MD (2012) Nomenclature of the amphibole super-group. Am Min 97:2031–2048
Hawthorne FC, Hughes JM, Cooper MA, Kampf AR (2022) Bonding between the decavanadate polyanion and the interstitial complex in pascoite-family minerals. Can Min 60:341–359
Huminicki DMC, Hawthorne FC (2002) The crystal chemistry of the phosphate minerals. In: Kohn MJ, Rakovan J, Hughes JM (eds) Phosphates: Geochemical, Geobiological, and Materials Importance, Reviews in Mineralogy and Geochemistry 48. Mineralogical Society of America, Washington DC, pp 123–253
Ingri N (1963) Equilibrium studies of polyanions containing B^{III}, Si^{IV}, Ge^{IV} and V^{V}. Svensk Kem Tidskr 75:3–34
Kampf AR, Hughes JM, Cooper MA, Hawthorne FC, Nash BP, Olds TA, Adams PM, Marty J (2021) The pascoite family of minerals, including the redefinition of rakovanite. Can Min 59:771–779
Kolesnikov AI, Reiter GF, Choudhury N, Prisk TR, Mamontov E, Podlesnyak A, Ehlers G, Seel AG, Wesolowski DJ, Anovitz LM (2016) Quantum tunneling of water in beryl: A new state of the water molecule. Phys Rev Lett 116:167802
Kolesnikov AI, Anovitz LM, Hawthorne FC, Podlesnyak A, Schenter GK (2019) Effect of fine-tuning pore structures on the dynamics of confined water. J Chem Phys 150:204706
Lovelock JE, Margulis L (1973) Atmospheric homeostasis by and for the biosphere: the gaia hypothesis. Tellus 26(1–2):2–10
Majzlan J, Plášil J, Dachs E, Benisek A, Koch CB (2016) Crystal chemistry, Mössbauer spectroscopy, and thermodynamic properties of botryogen. Neues Jb Miner Abh 193:147–159
Matthews PC (1998) Vector calculus. Springer, London
Mereiter K (1974) Die Kristallstruktur von Rhomboklas, $H_5O_2\{Fe[SO_4]_2{\cdot}2\ H_2O\}$. Tscher Miner Petrogr Mitt 21:216–232
Mihailova B, Della Ventura G, Waeselmann N, Xu W, Schlüter J, Galdenzi F, Marcelli A, Redhammer GJ, Boiocchi M, Oberti R (2021) Atomistic insight into lithospheric conductivity revealed by phonon-electron excitations in hydrous iron-bearing silicates. Commun Mater 2:57. https://doi.org/10.1038/s43246-021-00161-y
Mihailova B, Della Ventura G, Waeselmann N, Bernardini S, Xu W, Marcelli A (2022) Polarons in rock-forming minerals: physical implications. Condens Matter 7:68–80
Milovanović MR, Ivana M, Stanković IM, Živković JM, Ninković DB, Hall MB, Zarić SD (2022) Water: new aspect of hydrogen bonding in the solid state. IUCrJ 9:639–647
Oberti R, Boiocchi M, Zema N, Hawthorne FC, Redhammer GJ, Susta U, Della Ventura G (2018) The high-temperature behavior of riebeckite: expansivity, deprotonation, selective Fe oxidation and a novel cation disordering scheme for amphiboles. Eur J Min 30:437–449
Perrin DD (1965) Dissociation constants of inorganic acids and bases in aqueous solution. Butterworths, London
Peslier AH, Schönbächler M, Busemann H, Karato S-I (2017) Water in the Earth's interior: distribution and origin. Space Sci Rev 212:743–810
Preiser C, Lösel J, Brown ID, Kunz M, Skowron A (1999) Long range Coulomb forces and localized bonds. Acta Crystallogr B 55:698–711
Rahm M, Hoffmann R, Ashcroft NW (2017) Atomic and ionic radii of the elements. Chem Eur J 22:14625–14632
Rieder M, Cavazzini G, D'yakonov YS, Frank-Kamenetskii VA, Gottardi G, Guggenheim S, Müller G, Neiva AMR, Radoslovich EW, Robert JL, Sassi FP (1999) Nomenclature of the micas. Min Mag 63:267–296
Ripmeester JA, Ratcliffe CI, Dutrizac JE, Jambor JL (1986) Hydronium ion in the alunite-jarosite group. Can Min 24:435–447

Schindler M, Hawthorne FC (2001) A bond-valence approach to the structure, chemistry and paragenesis of hydroxy-hydrated oxysalt minerals: I. Theory. Can Min 39:1225–1242

Schindler M, Hawthorne FC (2004) A bond-valence approach to the uranyl-oxide hydroxy-hydrate minerals: Chemical composition and occurrence. Can Min 42:1601–1627

Schindler M, Hawthorne FC (2008) The stereochemistry and chemical composition of interstitial complexes in uranyl-oxysalt minerals. Can Min 46:467–501

Schindler M, Huminicki DMC, Hawthorne FC (2006) Sulfate minerals: I. Bond topology and chemical composition. Can Min 44:1403–1429

Smith JD, Cappa CD, Wilson KR, Cohen RC, Geissler PL, Saykally RJ (2005) Unified description of temperature-dependent hydrogen-bond rearrangements in liquid water. Proc Nat Acad Sci 102:14171–14174

Sokolova E, Hawthorne FC, Pautov LA, Agakhanov AA (2010) Byzantievite, Ba_5(Ca, REE, Y)$_{22}$(Ti, Nb)$_{18}$(SiO_4)$_4$[(PO_4),(SiO_4)]$_4$(BO_3)$_9$$O_{22}$[(OH), F]$_{43}$($H_2O$)$_{1.5}$; the crystal structure and crystal chemistry of the only known mineral with the oxyanions (BO_3), (SiO_4) and (PO_4). Min Mag 74:285–308

Stephens JS, Cruickshank DWJ (1970) The crystal structure of $(CrO_3)_\infty$. Acta Crystallogr B 26:222–226

Sutor DJ (1967) The crystal and molecular structure of newberyite, $MgHPO_4{\cdot}3H_2O$. Acta Crystallogr 23:418–422

Welch MD, Hawthorne FC, Cooper MA, Kyser TK (2001) Trivalent iodine in the crystal structure of schwartzembergite, $Pb^{2+}{}_5I^{3+}O_6H_2Cl_2$. Can Min 39:785–795

Wilkins RWT, Sabine W (1973) Water content of some nominally anhydrous silicates. Am Min 58:508–516

Wilson RJ (1979) Introduction to Graph Theory. Longman, London

Wood DL, Nassau K (1968) The characterization of beryl and emerald by visible and infrared absorption spectroscopy. Am Min 53:777–800